Single-Cell Transcriptional Profiling Reveals Signatures of Helper, Effector, and Regulatory MAIT Cells during Homeostasis and Activation

Charles Kyriakos Vorkas,[*,†,1,2] Chirag Krishna,[‡,1] Kelin Li,[§] Jeffrey Aubé,[§] Daniel W. Fitzgerald,[*,¶] Linas Mazutis,[‖] Christina S. Leslie,[‡,3] and Michael S. Glickman[†,#,3]

Mucosal-associated invariant T (MAIT) cells are innate-like lymphocytes that recognize microbial vitamin B metabolites and have emerging roles in infectious disease, autoimmunity, and cancer. Although MAIT cells are identified by a semi-invariant TCR, their phenotypic and functional heterogeneity is not well understood. Here we present an integrated single cell transcriptomic analysis of over 76,000 human MAIT cells during early and prolonged Ag-specific activation with the MR1 ligand 5-OP-RU and nonspecific TCR stimulation. We show that MAIT cells span a broad range of homeostatic, effector, helper, tissue-infiltrating, regulatory, and exhausted phenotypes, with distinct gene expression programs associated with $CD4^+$ or $CD8^+$ coexpression. During early activation, MAIT cells rapidly adopt a cytotoxic phenotype characterized by high expression of *GZMB*, *IFNG* and *TNF*. In contrast, prolonged stimulation induces heterogeneous states defined by proliferation, cytotoxicity, immune modulation, and exhaustion. We further demonstrate a FOXP3 expressing MAIT cell subset that phenotypically resembles conventional regulatory T cells. Moreover, scRNAseq-defined MAIT cell subpopulations were also detected in individuals recently exposed to *Mycobacterium tuberculosis*, confirming their presence during human infection. To our knowledge, our study provides the first comprehensive atlas of human MAIT cells in activation conditions and defines substantial functional heterogeneity, suggesting complex roles in health and disease. *The Journal of Immunology*, 2022, 208: 1–15.

Mucosal-associated invariant T (MAIT) cells are a subset of recirculating innate-like lymphocytes enriched in human liver, lung, and gut with highly variable abundance in peripheral blood in healthy donors (<1–18% in humans) (1–3). Most MAIT cells express an evolutionarily conserved TCR (TRAV1-2 in humans) that can recognize microbially derived, non-peptide small molecule metabolites of the vitamin B pathway (4, 5) presented by the oligomorphic MHC class Ib–related molecule, MR1 (5, 6). In contrast to conventional T cells that exit the thymus in a "naive" state and require peptide-specific Ag priming to proliferate, most mature MAIT cells enter the circulation as effector cells and are activated within hours of non-peptide vitamin B metabolite recognition (7, 8). This innate-like property confers their capacity to be among the first responders to bacterial and fungal pathogens (3, 9–11) as well as to viral infections through TCR-independent cytokine stimulation (12–14).

Despite a growing body of literature implicating MAIT cells in both homeostasis and disease (1), their specialized functional states in humans are poorly characterized relative to conventional T cells. For example, whereas conventional T cells are broadly divided into two lineages defined by CD4 or CD8 coreceptor expression and stable functional phenotypes, whether these same lineages can be

*Division of Infectious Diseases, Weill Cornell Medicine, Cornell University, New York, NY; †Immunology Program, Sloan Kettering Institute, Memorial Sloan Kettering Cancer Center, New York, NY; ‡Computational and Systems Biology Program, Sloan Kettering Institute, Memorial Sloan Kettering Cancer Center, New York, NY; §Division of Chemical Biology and Medicinal Chemistry, UNC Eshelman School of Pharmacy, University of North Carolina at Chapel Hill, Chapel Hill, NC; ¶Center for Global Health, Weill Cornell Medicine, Cornell University, New York, NY; ‖Single Cell Research Initiative, Sloan Kettering Institute, Memorial Sloan Kettering Cancer Center, New York, NY; and #Division of Infectious Diseases, Memorial Sloan Kettering Cancer Center, New York, NY

[1]C.K.V. and C.K. contributed equally to this work.

[2]Current address: Division of Infectious Diseases, Renaissance School of Medicine, Stony Brook University, Stony Brook, NY

[3]C.S.L. and M.S.G. are cosenior authors.

ORCIDs: 0000-0003-4952-7041 (C.K.V.); 0000-0002-8630-2928 (K.L.); 0000-0003-1049-5767 (J.A.); 0000-0002-5552-6427 (L.M.); 0000-0001-7918-5164 (M.S.G.).

Received for publication June 3, 2021. Accepted for publication December 9, 2021.

This work was supported by the Ludwig Center for Cancer Immunotherapy, the Tri-Institutional TB Research Unit, part of the Tuberculosis Research Units Network through National Institute of Allergy and Infectious Diseases Grant U19AI111143, and by National Cancer Institute Grants P30CA008748 and U54CA209975. L.M. acknowledges support by The Alan and Sandra Gerry Metastasis and Tumor Ecosystems Center. C.K.V. was supported by National Institute of Allergy and Infectious Diseases Grant K08AI132739 and a Potts Memorial Foundation Award.

BAM files and raw and normalized counts for all single-cell RNA sequencing data presented in this article have been submitted to Gene Expression Omnibus (https://www.ncbi.nlm.nih.gov/geo/query/acc.cgi?acc=GSE182239) under accession number GSE182239.

C.K.V. and M.S.G. conceived of the study. C.K.V. conducted the experiments and analyzed the flow cytometry data. J.A. and K.L. synthesized 5-A-RU. L.M. conducted inDROP scRNA-seq. D.W.F. recruited the Haitian TB contact cohort. C.K. and C.S.L. analyzed the scRNA-seq data. C.K.V., C.K., C.S.L., and M.S.G. curated the data and wrote the manuscript with input from all authors.

Address correspondence and reprint requests to Christina S. Leslie or Michael S. Glickman, 1275 York Avenue, Zuckerman 11th Floor, Computational and Systems Biology Program, Sloan Kettering Institute, Memorial Sloan Kettering Cancer Center, New York, NY 10065 (C.S.L.) or 1275 York Avenue, Box 477, Division of Infectious Diseases, Memorial Sloan Kettering Cancer Center, New York, NY 10065 (M.S.G.). E-mail addresses: cleslie@cbio.mskcc.org (C.S.L.) or glickmam@mskcc.org (M.S.G.)

The online version of this article contains supplemental material.

Abbreviations used in this article: 5-A-RU, 5-amino-6-D-ribitylaminouracil; C, cluster; DN, double-negative; DP, double-positive; FDR, false discovery rate; IGRA, IFN-γ release assay; MAIT, mucosal-associated invariant T; scRNA-seq, single-cell RNA sequencing; TB, tuberculosis; Treg, regulatory T cell; UMAP, uniform manifold approximation and projection.

defined in MAIT cells remains unclear. $CD4^+$ MAIT cells are reported to express increased CD25 and IL-2 along with decreased cytotoxic markers relative to $CD8^+$ MAIT cells (3, 12, 15, 16). Whereas $CD8^+$ and $CD4^-CD8^-$ [double-negative (DN)] MAIT cells have similar cytotoxic phenotypes (16), the DN subset is reported to have depressed function with increased propensity to activation-induced apoptosis (17). Although prior studies have suggested that MAIT cell functional states may depend on the quality and duration of activating stimuli (12, 18), the early and late effects of TCR stimulation on MAIT cell state remain largely unknown.

Although prior studies have described MAIT cell heterogeneity using flow cytometry or bulk RNA sequencing (9, 17, 19), such approaches are limited in resolution and likely do not capture the full extent of MAIT cell diversity in humans. Although some of these other studies have characterized MAIT cells together with other innate T cell populations at a modest scale with single-cell transcriptomics (19–22), a dedicated atlas of both $CD4^+$ and $CD8^+$ mature MAIT cells under various activation conditions in healthy human donors remains lacking. Indeed, recent reports of the importance of MAIT cells in cancer (23) and COVID-19 pathogenesis (24, 25) necessitate a large-scale single-cell atlas of MAIT cell heterogeneity stimulated with their cognate ligands.

In this study, we present a single-cell transcriptomic atlas of human MAIT cells, comprising >76,000 cells from peripheral blood under early and prolonged activation with 5-OP-RU or anti-CD3/CD28 in the presence of IL-2 or IL-2/TGF-β. Our study elucidates distinct transcriptional programs of $CD4^+$ and $CD8^+$ MAIT cells and identifies novel MAIT cell functional clusters that we validate in human subjects recently exposed to *Mycobacterium tuberculosis*. Our results demonstrate broad functional heterogeneity of MAIT cells and suggest that these innate T cells can participate in complex immune responses in addition to their role in direct killing of pathogens.

Materials and Methods

PBMC collection

Healthy donor PBMCs were obtained with written informed consent at Sloan Kettering Institute, Memorial Sloan-Kettering Cancer Center, Rockefeller University, or ATCC. De-identified blood samples were processed according to the protocols approved by the Institutional Review Board of Memorial Sloan-Kettering Cancer Center and Rockefeller University. As PBMC samples were de-identified, no demographic or clinical information is available. Tuberculosis (TB) household contacts and unexposed community controls were recruited with written informed consent at the GHESKIO centers, Port-au-Prince, Haiti (U01AI069421). Demographic and clinical variables of this cohort were previously described (3). Sample sizes for each experiment are described in the main text and figure legends. PBMCs were isolated from peripheral blood using Ficoll-Prep (GE Healthcare) or cell preservation tubes (Becton Dickinson) according to the manufacturer's instructions and cryopreserved using 90% FBS (Life Technologies)/10% DMSO (Sigma-Aldrich) and stored in liquid N_2 prior to thawing for in vitro assays.

PBMC culture

PBMCs were cultured for 15 h or 7 d in RPMI 1640 (Life Technologies) supplemented with 10% (v/v) heat-inactivated FBS, penicillin/streptomycin (100 U/ml), L-glutamine (2 mM), sodium pyruvate (1 mM), nonessential amino acids (0.1 mM), HEPES buffer (10 mM), and 2-ME (50 μM) (from Life Technologies or Sigma-Aldrich) at 37°C, 5% CO_2 in 96-well plates in the presence of IL-2 [Life Technologies (100 IU/ml) or Roche (1 ng/ml)]. Additional conditions included 1 ng/ml TGF-β (Life Technologies). Two micromolar 5-amino-6-D-ribitylaminouracil (5-A-RU) was added directly to 50 μM methylglyoxal to form 5-OP-RU on day 1 for in vitro stimulation assays. 5-A-RU was synthesized as previously described (2), resuspended in 200 μM aliquots, cryopreserved, and thawed as needed. Anti-CD3/CD28 beads (Life Technologies, 11161D) were incubated with PBMCs at a 1:2 bead/cell ratio for single-cell RNA sequencing (scRNA-seq) and flow cytometric validation assays. Refer to the Table I for a complete list of cell culture reagents.

Flow cytometry

Cells were washed once in FACS buffer then incubated with Fc receptor binder inhibitor polyclonal Abs (eBioscience, 14-9161-73) for 15 min at room temperature prior to staining. Extracellular staining was performed at room temperature for 15 min in 50 μl of FACS buffer (eBioscience, 00-4222-26), whereas intracellular staining was performed after 2 h of incubation in brefeldin A at 37°C followed by 45 min of incubation in 50 μl of permeabilization/fixation buffer (eBioscience; Foxp3/transcription factor staining buffer kit, 00-5523-00) followed by incubation for 1 h in 50 μl permeabilization buffer at 4°C. Refer to Table I for a complete list of Abs and flow cytometry reagents.

Cell barcoding and scRNA-seq library preparation

The FACS-sorted live-cell suspensions were encapsulated in microfluidic droplets using a Chromium instrument (10× Genomics) and reagents provided in a Single Cell 3′ Reagent kit (v3). The barcoded cDNA libraries were prepared according to the manual (CG00183 rev. B). The viability of cells [stained with 0.2% (w/v) trypan blue] prior to loading onto the Chromium instrument was 80–98%. Each sample was encapsulated at a final dilution of ~100 cells/μl. Following the reverse transcription step, the emulsion droplets were broken and barcoded cDNA was purified with Dynabeads and amplified by 12 cycles of PCR: 98°C for 180 s, 12 times (98°C for 15 s, 67°C for 20 s, 72°C for 60 s), and 72°C for 60 s. The 50 ng of PCR-amplified barcoded cDNA was fragmented with the reagents provided in the kit, purified with SPRI beads, and resulting DNA library was ligated to the sequencing adapter followed by indexing PCR: 98°C for 45 s, 14 times (98°C for 20 s, 54°C for 30 s, 72°C for 20 s), and 72°C for 60 s. The final DNA library was double-size purified (0.6–0.8×) with SPRI beads and sequenced on the Illumina Nova-Seq platform (R1, 26 cycles; i7, 8 cycles; R2, 70 or more cycles) at a depth of 220 million reads per sample. BAM files and raw and normalized counts for all single-cell RNA sequencing data presented in this article have been submitted to Gene Expression Omnibus (https://www.ncbi.nlm.nih.gov/geo/query/acc.cgi?acc=GSE182239) under accession number GSE182239.

Quantification and statistical analysis

Flow-assisted cell sorting and flow cytometric analysis. The flow cytometric gating strategy to identify MAIT cells using MR1-5-OP-RU tetramers generated by the National Institutes of Health tetramer core facility (2, 26) is summarized in Supplemental Fig. 1. The percentage of MAIT cells of total $CD3^+$ cells and the absolute number of cells sorted per condition are presented in Supplemental Table I. Stained cells were sorted on a BD FACSAria sorter or analyzed on a BD LSRFortessa analyzer. Flow cytometry plots and analysis were performed using FCS Express version 7 (De Novo Software, Pasadena, CA). Graphs and statistical analysis of flow cytometry data were generated using Prism version 11 software (GraphPad Software, San Diego, CA). Absolute numbers were analyzed for experiments when the initial cell number per well was identical for each donor (200,000 PBMCs/well). Otherwise, the relative frequencies (%) are reported. Paired t tests, unpaired t tests, and Mann–Whitney tests were used to determine statistical significance between incubation conditions. Level of significance was $p < 0.05$. Adjusted p values for multiple t test comparisons were calculated by the Holm–Sidak method.

scRNA-seq analysis. Preprocessing of scRNA-seq fastq files was conducted using the seqc pipeline as previously described (27). Following count matrix generation, cells with >20% of transcripts derived from mitochondrial genes were considered apoptotic and were thus excluded, consistent with prior work (27). Following this step, all mitochondrial genes were filtered out of the count matrix. Ribosomal genes and the noncoding RNAs NEAT1 and MALAT1 were excluded due to prior reports of strong influence on downstream clustering. Genes with a mean raw count <3.0 were removed from the analysis, and we restricted to $KLRB1^+$ cells, which are a marker of MAIT cell lineage, and defined our FACS-sorting strategy for additional quality control, resulting in a final count matrix of 76,945 cells and 12,499 genes for downstream analysis. We used Seurat v2.3.4 to perform standard library size and log normalization. The mean library size was 6680 transcripts per cell.

To examine potential batch effects in the data (28), we computed the prevalence of each cluster out of all cells in each sample, followed by a centered log-ratio transformation for compositional data and principal-component analysis. This analysis demonstrated that samples clustered by time point, not batch (i.e., donor) (Supplemental Fig. 1E). Furthermore, pairwise Euclidean distances between samples from day 1 and day 7 were higher than pairwise distances within each time point (Supplemental Fig. 1F). When attempting batch correction, we detected no differences between cluster phenotypes at day 1

Table I. Reagents and resources

Reagent or Resource	Source	Identifier
Abs		
FITC granzyme B (clone GB11)	BioLegend	Cat#515403; RRID:AB_2114575
BUV395 Ki67 (clone B56)	BD	Cat#564071; RRID:AB_393778
PE-Cy7 FOXP3 (clone PHC101)	eBioscience	Cat#25-4776-42; RRID:AB_10804638
PE IFN-γ (clone B27)	BioLegend	Cat#506507; RRID:AB_315440
BV785 IFN-γ (clone 4S.BS3)	BioLegend	Cat#502542; RRID:AB_2563882
BV605 TNF-α (clone Mab11)	BioLegend	Cat#502936; RRID:AB_2563884
BV711 CD25 (clone BC96)	BioLegend	Cat#302636; RRID:AB_2562910
PerCP-Cy5.5 OX40 (clone Ber-ACT35)	BioLegend	Cat#350010; RRID:AB_10719224
Allophycocyanin CD161 (clone DX12)	BD	Cat#550968; RRID:AB_398482
BV650 (clone DX12)	BD	Cat#563864; RRID:AB_2738456
Alexa Fluor 700 (clone UCHT1)	BD	Cat#557943; RRID:AB_396952
Allophycocyanin-Cy7 CD8 (clone SK1)	BD	Cat#560179; RRID:AB_1645481
BUV737 CD8 (clone SK1)	BD	Cat#564269; RRID:AB_2870085
PerCP-eFluor 710 CD4 (clone SK3)	eBioscience	Cat#46-0047-42; RRID:AB_1834401
BUV496 CD4 (clone SK3)	BD	Cat#564651; RRID:AB_2744422
eFluor 660 EOMES (clone WD1928)	eBioscience	Cat#50-4877-42; RRID:AB_2574229
PE-Cy5 CTLA4 (clone BNI3)	BD	Cat#555854; RRID:AB 396177
Pacific Blue granzyme A (clone CB9)	BioLegend	Cat#507207; RRID:AB_439755
PerCp-Cy5.5 granzyme K (clone GM26E7)	BioLegend	Cat#370514; RRID:AB_2632852
BUV395 IL-7R (clone HIL-7R-M21)	BD	Cat#742547; RRID:AB_2740857
BV421 CD69 (clone FN50)	BioLegend	Cat#310930; RRID:AB_2561909
PerCP-eFluor CD69 (clone FN50)	BD	Cat#46-0699-42; RRID:AB_2573694
PerCP-eFluor ICOS (clone ISA-3)	eBioscience	Cat#46-9948-42; RRID:AB_10854730
BV510 FAS (clone DX2)	BioLegend	Cat#305640; RRID:AB_2629738
BV421 LAG3 (clone 11C3C65)	BioLegend	Cat#369314; RRID:AB_2629797
BV650 PD-1 (clone EH12.2H7)	BioLegend	Cat#329950; RRID:AB_2566362
BV510 CCR7 (clone 3D12)	BD	Cat#563449; RRID:AB_2738212
Fc receptor binding inhibitor polyclonal Ab	eBioscience	Cat#14-9161-73; RRID:AB_468582
Purified anti-human MR1 (clone 26.5)	BioLegend	Cat#361102; RRID:AB_2562969
Chemicals, peptides, and recombinant proteins		
5-amino-6-D-ribitylaminouracil (5-A-RU)	Aubé laboratory, UNC	https://pharmacy.unc.edu/directory/jaube/
Methylglyoxal	Sigma-Aldrich	Cat#M0252-25ML
Recombinant human IL-2	Life Technologies	Cat#PHC0021
Recombinant human IL-2	Roche	Cat#HIL2-RO
Recombinant human TGF-β1	Life Technologies	Cat#PHG9204
Penicillin/streptomycin	Life Technologies	Cat#15-140-122
RPMI 1640	Life Technologies	Cat#21870092
L-Glutamine	Life Technologies	Cat#25030149
FBS	Life Technologies	Cat#26140079
RPMI 1640	Life Technologies	Cat#21870092
HEPES	Life Technologies	Cat#15630080
Sodium pyruvate	Life Technologies	Cat#11360070
MEM nonessential amino acids	Life Technologies	Cat#11140050
Flow cytometry staining buffer	eBioscience	Cat#00-4222-26
Foxp3/transcription factor staining buffer set	eBioscience	Cat#00-5523-00
2-ME	Sigma-Aldrich	Cat#M6250-250ML
Critical commercial assays		
FITC annexin V apoptosis detection kit	Invitrogen	Cat#88-8005-72
PerCP-eFluor 710 annexin V apoptosis detection kit	Invitrogen	Cat#88-8008-72
Dynabeads human T-activator CD3/CD28	Life Technologies	Cat#11161D
Biological samples		
Healthy human PBMCs	Memorial Sloan-Kettering Cancer Center, Rockefeller University, ATCC	N/A
Healthy human TB contact/control PBMCs	GHESKIO Centers	N/A
Deposited data		
Raw and analyzed data	This paper	GEO accession: GSE182239
Software and algorithms		
Cell Ranger	v3.0.2	https://github.com/10XGenomics/cellranger
Seurat	v2.3.4	https://satijalab.org/seurat/articles/install.html
R	v3.6.1	https://www.r-project.org/
FCS express v7	De Novo Software	https://denovosoftware.com/
Prism v11	GraphPad Software	https://www.graphpad.com/scientific-software/prism/
Other		
PE or BV421 MR1-5OPRU/6FP tetramers	NIH Tetramer Core Facility	https://tetramer.yerkes.emory.edu/reagents/mr1

BD, BD Biosciences; Cat#, catalog number; N/A, not applicable.

and day 7, a result inconsistent with prior studies showing differences between MAIT cells in response to stimulation at early and late time points. We further found that "overcorrection" of the data introduced spurious batch effects, for example, clustering of donor rather than time point. Therefore, we proceeded to analyze the data without batch correction.

Differential expression analyses were conducted using the FindMarkers() function in Seurat using a Wilcoxon test. Specifically, we compared each cluster to all other clusters (one versus all), and genes were considered signature genes for a cluster when the log fold change was >0 and the false discovery rate (FDR)–adjusted p was ≤0.05.

Signature enrichment analyses. Signatures for conventional immune cells were derived from Bindea et al. (29). Signatures were also manually curated from the Kyoto Encyclopedia of Genes and Genomes and Reactome databases. For analyses in Supplemental Fig. 2, significantly differentially expressed genes for each cluster were used as input to the fgsea() package in Bioconductor. Associations were considered significant at a FDR-adjusted p of ≤0.05.

Results

CD4 or CD8 expression on MAIT cells is associated with distinct transcriptional states

To simulate early and prolonged MAIT cell activation under Ag-specific and nonspecific TCR stimulation, we employed an in vitro activation assay using human PBMCs incubated with MR1 ligand (5-OP-RU) or anti-CD3/CD28 beads for 15 h (day 1; early) or 7 d (day 7; prolonged) compared with unstimulated control cells. As MR1-expressing cells such as B cells and monocytes are abundant within PBMCs, they can directly present 5-OP-RU to MAIT cells (2, 30, 31). A subset of conditions at day 7 also included TGF-β to further assess potential regulatory phenotypes (32, 33). Cells were harvested at each time point for flow cytometric assays and FACS using MR1 tetramers (Fig. 1A, Supplemental Fig. 1A–C, Supplemental Table I). To define the transcriptional landscape of MAIT cell states after early and prolonged activation, we performed droplet microfluidics scRNA-seq of these sorted MAIT cells from the peripheral blood of three donors in the activation conditions defined above. In total, 76,945 MAIT cells passed quality control and were used for downstream analysis (Supplemental Table I).

Although prior studies have demonstrated that MAIT cells can express CD4 or CD8 coreceptors (3, 15, 16), it is unclear whether these markers define functionally distinct MAIT cell populations. To address this question, we sequenced all MAIT cells per condition by sorting total $CD3^+$MR1-5-OP-RU $tetramer^+CD161^{++}$ populations (Supplemental Fig. 1A–C) and included incubation conditions favoring MAIT cell expansion in vitro (Supplemental Fig. 1B), so as to enrich for rarer MAIT cell subsets (e.g., $CD4^+$ subset). Representative staining of $CD4^+$/$CD8^+$ coexpressing MAIT cell subsets are included in Supplemental Fig. 1D.

To test the hypothesis that $CD4^+$ and $CD8^+$ MAIT cells are composed of distinct transcriptional lineages, we first performed a differential expression analysis of our single-cell data set to compare $CD4^+CD8^-$ and $CD4^-CD8^+$ MAIT cells at day 1 (Fig. 1B, 1C) or day 7 (Fig. 1D, 1E) in the absence of TCR stimulation (Supplemental Data Set 1). At day 1 (Fig. 1C) $CD4^+$ MAIT cells highly express genes associated with conventional naive and central memory T cells, including *LEF1*, *SELL*, and *CCR7*, but also markers of activation and costimulation such as *CTLA4*, *IL2RA*, *TNFRSF4*, and *TNFRSF18* (Fig. 1B). In contrast, $CD8^+$ MAIT cells express markers of cytotoxic activity such as *NKG7*, *KLRD1*, *EOMES*, *GNLY*, and *GZMB* as well as the transcription factor *RORA*. We confirmed the differential expression of CD25, OX40, GZMB, and EOMES at the protein level within $CD4^+$, $CD8^+$, DN, and $CD4^+CD8^+$ [double-positive (DP)] MAIT cell subsets using flow cytometry (Fig. 1C). At day 7, $CD4^+$ MAIT cells upregulated *CTLA4*, *TNFRSF4*, *SELL*, *IL2RA*, and *CCR7*, whereas $CD8^+$ MAIT cells upregulated *NKG7*, *GZMA*, *GZMK*, *PRF1*, and SLAMF7 as well as several genes involved in type 1 IFN signaling (*IFI44L*, *IFITM3*, *IFI6*, *IFITM1*, and *ISG15*) (Fig. 1D). We also confirmed the differential expression of OX40, CTLA4, GZMA, and GZMK in each subset at the protein level by flow cytometry (Fig. 1E). Our analysis demonstrates that $CD4^+$ MAIT cells are associated with expression of costimulatory receptors, IL-2 signaling, and memory markers, whereas $CD8^+$ MAIT cells are defined by granzyme-mediated cytotoxicity and type 1 IFN signaling. These results suggest that CD4 and CD8 expression on MAIT cells may define distinct functional subpopulations.

Single-cell transcriptional analysis defines heterogeneous MAIT cell activation states

To fully characterize the phenotypic states of MR1-5-OP-RU $tetramer^+CD161^{++}$ cells, we performed dimensionality reduction by principal-component analysis followed by Louvain clustering on cells from all donors, time points, and stimuli (Fig. 2A, Supplemental Data Set 2). Integration of all samples across all time points revealed that clusters were broadly partitioned by time point rather than donor (Supplemental Fig. 1E), consistent with earlier studies of both conventional T cells and MAIT cells demonstrating transcriptional changes over time in response to stimulation (1, 14, 18, 34–38). Accordingly, distances between samples within a time point were far lower than distances between samples from different time points, lending confidence to our integration approach (Supplemental Fig. 1F). In addition, samples from each donor were largely overlapping, with more heterogeneity observed by stimulus (Supplemental Fig. 1G) or time point (Supplemental Fig. 1H, 1I). Visualization with uniform manifold approximation and projection (UMAP) together with differential expression analysis displayed 12 clusters that could be distinguished by homeostatic, cytotoxic, Th1 helper–associated cytokine release, proliferating, tissue-infiltrating, immune regulatory, and exhausted states (Fig. 2B, 2C, Supplemental Data Set 2). Clusters (C)1–C3 were enriched at day 1 (early activation; Fig. 2D, Supplemental Data Set 2). C1 had high expression of *IFNG*, *GZMB*, *TNF*, *TBX21*, and notably the transcription factor *FOXP3*. Because this cluster expressed genes associated with granzymes and Th1 helper–associated cytokines, it was termed "MAIT1 cytotoxic effector," consistent with a similar cluster detected in Koay et al. (21). C2 demonstrated increased *CD69* and pronounced expression of heat shock proteins, *NR4A1*, and the AP-1 subunits *JUN* and *FOS* and was named "early activated." C3 expressed effector/central memory markers *CCR7* and *C62L*, markers of MAIT cell intrathymic development *CD4* and *LEF1* (21), as well as *RUNX3*. This cluster also upregulated type 1 IFN signaling genes, e.g., *IFIT3* and *ISG15*. Thus, C3 was named "ISG^+ memory" [after IFN-stimulated genes [ISGs]). Collectively, these clusters define the landscape of MAIT cells during homeostasis and early activation. The rapid induction of cytotoxic effector programs at this time point suggests that MAIT cells may be poised to respond earlier than conventional T cells.

In contrast, C4–C12 were enriched with prolonged activation and demonstrated marked phenotypic heterogeneity (Fig. 2E, Supplemental Data Set 2). C4 and C5 ("homeostatic effectors") displayed similar expression patterns, with high levels of *IL7R*, *GZMM*, *GZMK*, *KLRG1*, and *IFI44L* and decreased expression of *CD69* and *CD25*. C4 was distinguished from C5 by expression of vascular endothelial growth factors *VEGFA/B* and was named "homeostatic effector VEGF." C6 (degranulating effector") showed high expression of *LAMP1*, cytokines *TNF* and *TNFSF13B* (B cell activating factor), *IFNGR1*, as well as the homing molecule *CXCR3*. C7 ("$MR1^+$ MAIT17") expressed *GZMA*, *ENTPD1*, *RORA* (21), as well as *MR1* itself, suggesting that this population may interact with other MAIT cells. C8 ("tissue-infiltrating-like") highly expressed *ITGA1* and *ITGAE* and was only present in activation conditions including TGF-β. C9 was termed "innate-like" given its high expression of *HOPX*, *KLRB1*, and *NCR3* together with *GZMA* and

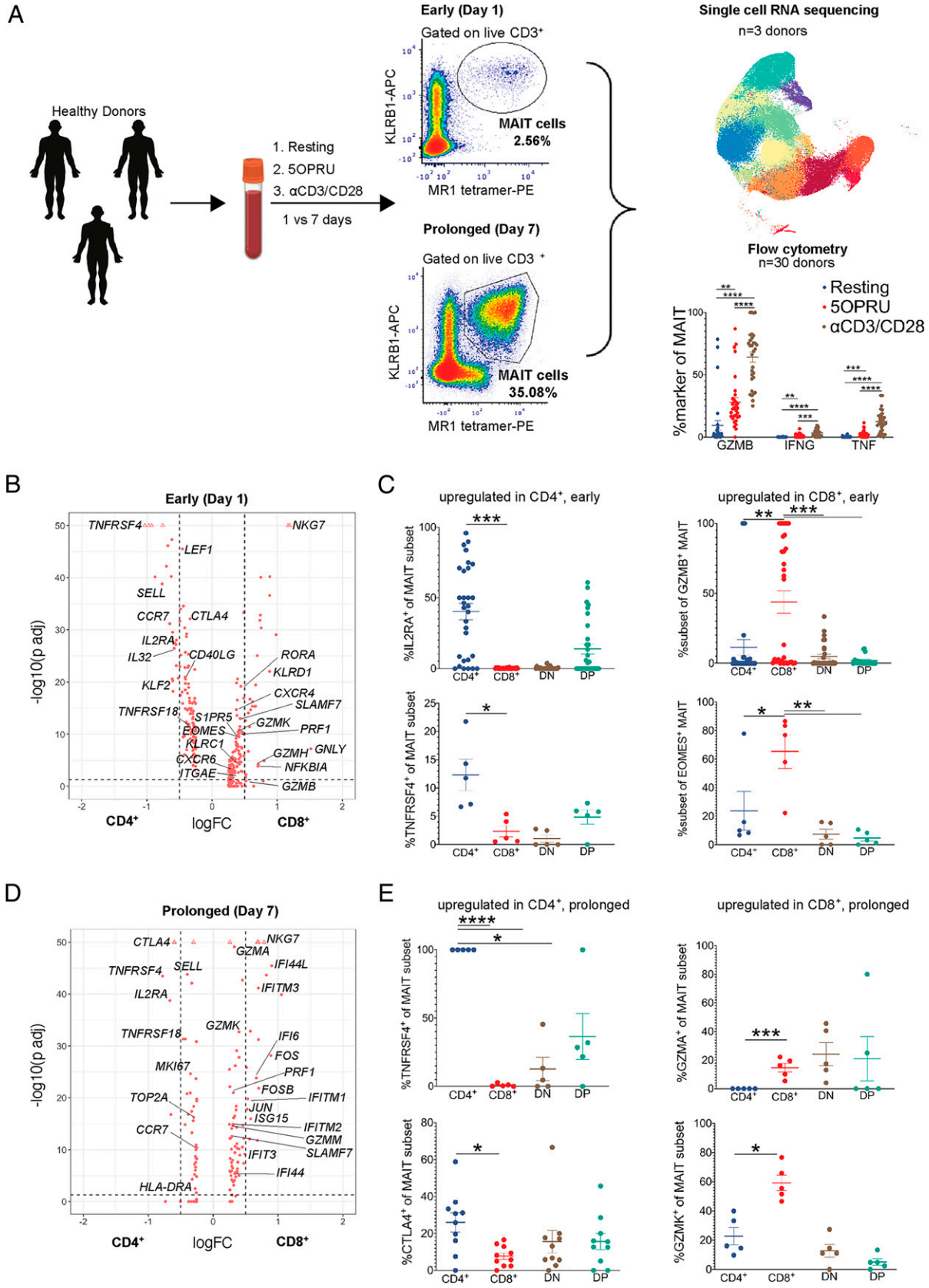

FIGURE 1. MAIT cell CD4 or CD8 expression levels are associated with distinct transcriptional signatures. (**A**) Experimental schematic of the MAIT cell in vitro activation assay used for single-cell RNA sequencing (scRNA-seq) and flow cytometric analyses. A total of 30 healthy donor PBMCs were assayed by flow cytometry after 15 h (day 1; early activation) or 7 d (day 7; prolonged activation) of incubation under resting, 5-OP-RU, or anti-CD3/CD28 conditions. A subset of three of these donors underwent FACS for scRNA-seq under the same conditions. All conditions included IL-2 and a subset of day 7 conditions also included TGF-β. (**B**) Differentially expressed genes in $CD8^+$ [+ log fold change (FC)] or $CD4^+$ MAIT cells (− log FC) after 15 h of incubation in the resting condition. The *y*-axis shows log FDR-adjusted *p* value with a significance level of FDR-adjusted $p < 0.05$. (**C**) Mean % ± SEM of CD25, OX40, GZMB, and EOMES staining in $CD4^+$, $CD8^+$, DN, or DP MAIT cell subsets measured by flow cytometry in the same *(Figure legend continues)*

GZMK. C10–C12 were defined by a gradient of activation/exhaustion marker expression including *CTLA4*, *PDCD1*, and *LAG3*, with C12 ("late activated/exhausted") resembling a terminally exhausted population. C11 ("proliferating") demonstrated a strong mitotic phenotype. C10 ("cytotoxic/regulatory") upregulated *GZMA*, *GNLY*, and *IL26* as well as immune-modulating genes *TGFB* and *LAG3*. Taken together, these analyses define a highly diverse MAIT cell transcriptional landscape shaped by prolonged activation, with important parallels with conventional $CD4^+$ and $CD8^+$ T cells.

We next asked to what extent previously published markers associated with mouse and human MAIT cells identified in key prior studies (39–41) are represented within the heterogeneous collection of MAIT clusters we present in the current study. We thus analyzed a wide array of transcription factors, cytokines/chemokines and their receptors, effector molecules, NK receptors, and other markers previously shown to be expressed on MAIT cells, and plotted them on top of our clusters (Supplemental Fig. 2A). We detected expression of key transcription factors IKZF2, RORC, and EOMES as well as the chemokines CCR2, CCR5, and CXCR6 in clusters also expressing CD8. In contrast, $CD4^+$ clusters demonstrated expression of IL2RA, CCR7, and SELL expression, consistent with our analysis directly comparing $CD4^+$ with $CD8^+$ MAIT cells (Fig. 1B).

We further asked whether markers typically associated with conventional $CD4^+$ and $CD8^+$ T cell subpopulations are expressed in MAIT cells (Supplemental Fig. 2B). We therefore manually curated markers that define key conventional T cell lineages that were not already represented in the heatmap in Supplemental Fig. 2A. This analysis revealed that FOXP3 was strongly expressed in C1, which also differentially expressed CD4. Moreover, we observed expression of key transcription factors that define the ontogeny and activation of conventional T cell lineages, for example, STAT1, RUNX3, PRDM1 (BLIMP1), and GATA3. We also found differential expression of activation/exhaustion markers, for example, HAVCR2 (TIM3), CTLA4, and PD1, in clusters where CD8 was differentially expressed. Consistent with this idea, we performed an additional pathway analysis using signatures of immune populations derived in Bindea et al. (29). This analysis revealed enrichment of NK and $CD4^+$/$CD8^+$ T cell signatures within our clusters, including differential enrichment of Th1 helper, Th2, central memory, and effector memory phenotypes (Supplemental Fig. 2C). We also performed pathway analyses using curated databases from Kyoto Encyclopedia of Genes and Genomes and Reactome (Supplemental Fig. 2D, 2E) that revealed enrichment of various antiviral immune response pathways (e.g., NOD-like receptor signaling), general effector pathways (e.g., TNF signaling), and pathways related to Ag presentation, for example, MHC class II protein complex binding. Given the recent association of MAIT cell responses with severity of SARS-CoV-2 infection, we also plotted markers of cytotoxicity found in patients with severe disease (25) on our clusters (Supplemental Fig. 2F). A subset of markers associated with severe COVID-19 disease were significantly upregulated in our clusters (Supplemental Fig. 2F). Specifically, GNLY (C3 and C10–C12), PRDM1 (C1, C2, C7, and C12), and IFITM1 (C3 and C12) were significantly differentially expressed in day 1 and day 7 clusters, whereas TXNIP (C4–C6) was more highly expressed in day 7 clusters. Taken together, we show that $CD4^+$ and $CD8^+$ MAIT cell subsets are transcriptionally distinct and can adopt similar programs to innate lymphocytes and conventional T cells.

Early MAIT cell activation induces a cytotoxic phenotype marked by GZMB, IFNG, *and* TNF

We next asked how the prevalence of these populations varied across stimuli and donors during early and prolonged activation (Fig. 2D, 2E, Supplemental Fig. 1H, and 1I). In particular, C1 MAIT1 cytotoxic effector—which expressed high levels of *IFNG*, *GZMB*, and *TNF*—was enriched by TCR stimulation conditions with 5-OP-RU or anti-CD3/CD28 compared with cells incubated with IL-2 alone (Fig. 3A, 3B). To validate these early transcriptional phenotypes, we performed flow cytometric characterization of MAIT cells under the same early activation conditions, which confirmed the differential expression of common T cell surface activation markers IL-7R, CD69, and CD25 (Fig. 3C). Unexpectedly, IL-7R was significantly downregulated by 5-OP-RU, but not anti-CD3/CD28. CD69 and CD25 were significantly upregulated by both stimulation conditions, although CD69 was more highly expressed with anti-CD3/CD28. To confirm that these phenotypes were not driven by activation-induced apoptosis, we stained with early activation/apoptosis marker annexin V and late apoptosis marker, activated caspase-3/7 (Supplemental Fig. 3). Whereas annexin V staining was increased by 5-OP-RU or anti-CD3/CD28 stimulation (Supplemental Fig. 3A), no difference in caspase staining was observed between resting and 5-OP-RU conditions (Supplemental Fig. 3B–E). This suggests that the increased annexin V staining observed represents early activation rather than apoptosis (42). In sum, these results demonstrate that MAIT cells rapidly adopt distinct immune phenotypes after early Ag-specific and nonspecific TCR stimulation.

As *GZMB*, *IFNG*, and *TNF* were significantly upregulated in early activation C1 and C2, we next asked whether these markers were coexpressed at the protein level. A representative gating strategy of intracellular costaining for GZMB, IFNG, and TNF is presented alongside cumulative data from 30 healthy donors (Fig. 3D). These analyses confirmed the presence of a MAIT cell population with a combined granzyme and Th1 helper–associated cytokine phenotype enriched with early activation, consistent with MAIT1 cytotoxic C1 enriched in the anti-CD3/CD28 condition in the scRNA-seq analysis. The primary early activation response in MAIT cells was upregulation of granzyme B alone, which was increased in anti-CD3/CD28 relative to 5-OP-RU conditions (Fig. 3D). 5-OP-RU and anti-CD3/CD28 both induced significant coexpression of GZMB and TNF, although increased coexpression was observed with anti-CD3/CD28 (Fig. 3D). Only anti-CD3/CD28 induced IFNG and TNF coexpression (Fig. 3D). These results demonstrate increased expression of IFNG and TNF with nonspecific TCR stimulation, consistent with previous reports (3, 12, 43).

We next performed a differential expression analysis between MAIT cells stimulated with 5-OP-RU and anti-CD3/CD28 at day 1 to define the gene expression programs associated with Ag-specific or nonspecific TCR stimulation (Fig. 3E, Supplemental Data Set 3). Although both early TCR stimulation conditions induced similar

condition as (B). Represents three independent experiments. $n = 5–30$ donors. (**D**) Differentially expressed genes in $CD8^+$ or $CD4^+$ MAIT cells after 7 d of incubation in the resting condition. Same axes as panel B. (**E**) Mean % ± SEM of OX40, CTLA4, GZMA, and GZMK staining in MAIT cell subsets measured by flow cytometry in the same condition as (D). Represents two independent experiments. $n = 5–10$ donors. Flow cytometric statistical comparisons were made by an unpaired t test, and reported p values are adjusted for multiple comparisons using the Holm–Sidak method. $*p < 0.05$, $**p < 0.005$, $***p < 0.0005$, $****p < 0.0001$. DN, double-negative ($CD4^-CD8^-$); DP, double-positive ($CD4^+CD8^+$); GZMA, granzyme A; GZMB, granzyme B; GZMK, granzyme K.

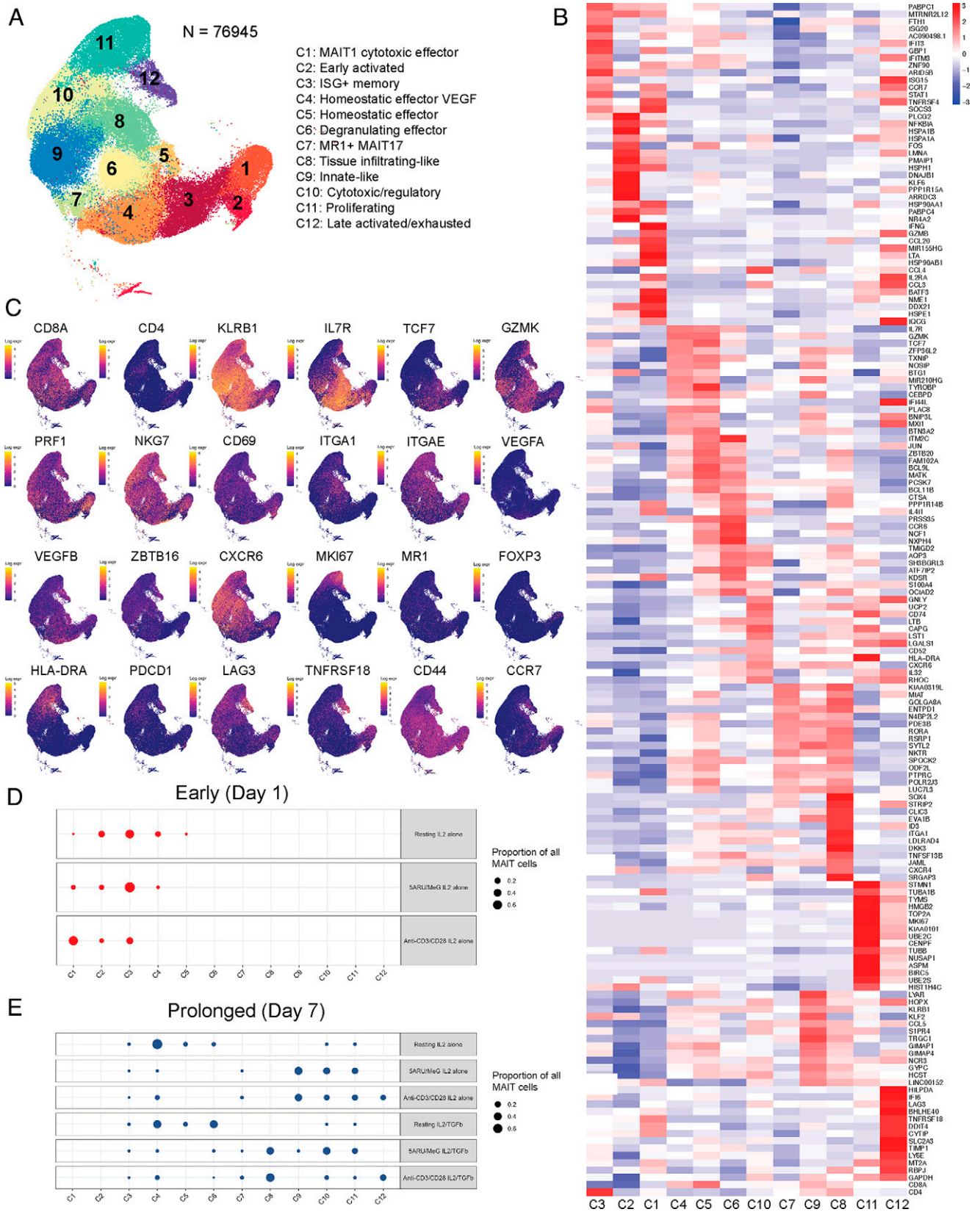

FIGURE 2. Single-cell transcriptional analysis defines heterogeneous MAIT cell activation states. (**A**) UMAP plot and Louvain clustering of cells from all donors, time points and stimuli with ascribed names based on differentially expressed gene sets in each cluster. (**B**) Heat map showing top 15 differentially expressed genes per cluster after unsupervised hierarchical clustering. (**C**) UMAP plots of selected MAIT cell markers demonstrating expression level across all clusters (blue = low expression to yellow = high expression). (**D** and **E**) Dot plots demonstrating relative frequency of cells per condition in all donors at day 1 (D) and day 7 (E).

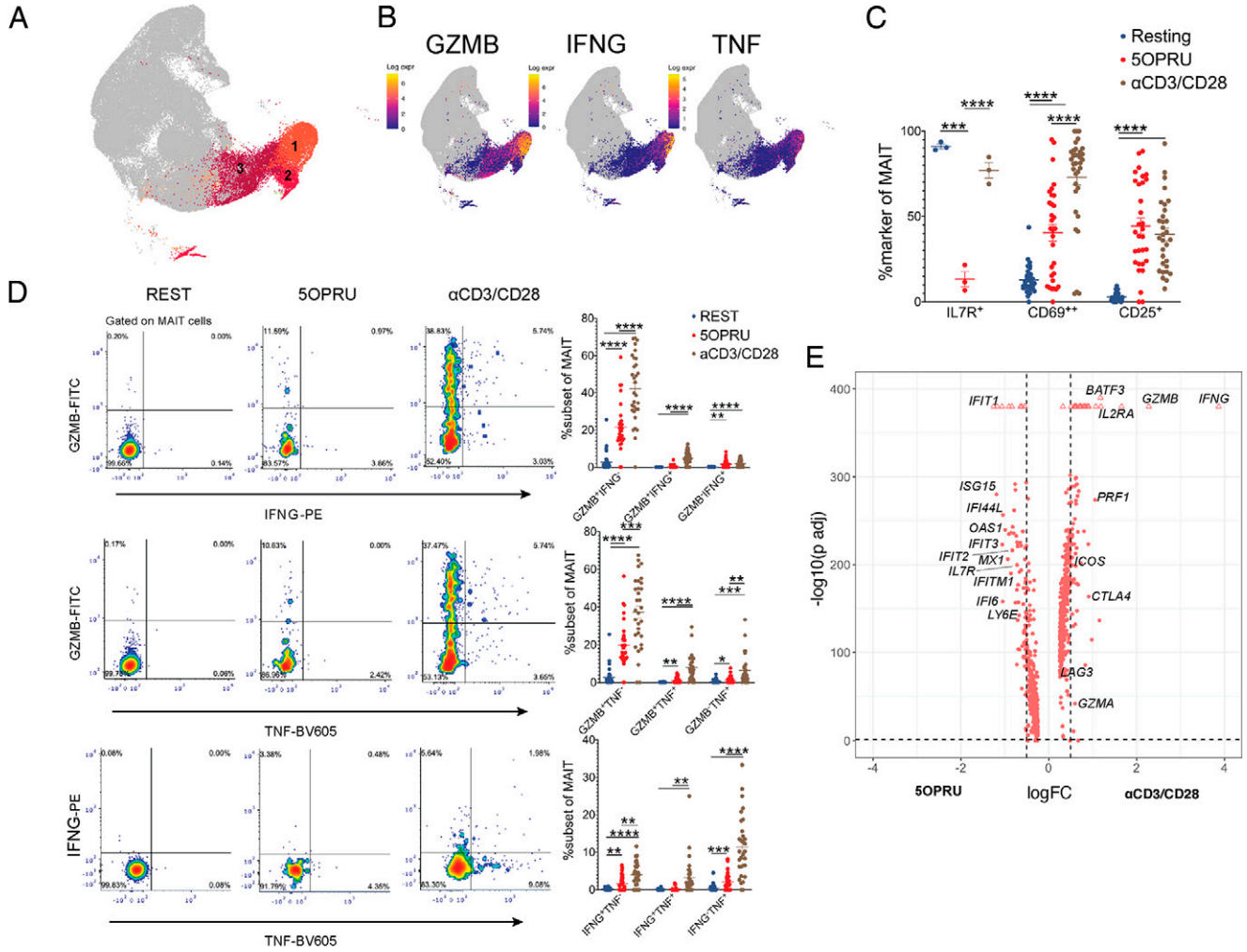

FIGURE 3. Early MAIT cell activation induces a cytotoxic phenotype marked by GZMB, IFNG, and TNF. (**A**) UMAP plot highlighting clusters 1–3 enriched in day 1 incubation conditions. (**B**) UMAP plots of GZMB, IFNG, and TNF expression levels at day 1 (blue = low expression to yellow = high expression). (**C**) Mean % ± SEM of MAIT cell extracellular staining of activation markers detected by flow cytometry after 15 h of incubation in three conditions: resting (blue), 5-OP-RU (red), anti-CD3/CD28 (brown). Results represent four independent experiments. n = 3–30 donors. (**D**) Representative flow cytometry density plots in one donor demonstrating GZMB, TNF, and IFNG costaining (left) alongside cumulative plots (right) of mean % ± SEM for each costaining condition in multiple donors. Results represent four independent experiments. n = 30 donors. (**E**) Differentially expressed genes in the anti-CD3/CD28 (+ log FC) or 5-OP-RU (− log FC) conditions at day 1. The y-axis shows log FDR-adjusted p value at significance level of FDR-adjusted $p < 0.05$. Triangles represent genes for which adjusted p values have been capped only for display on the plot. Flow cytometric statistical comparisons were made by an unpaired t test, and reported p values are adjusted for multiple comparisons using the Holm–Sidak method. *$p < 0.05$, **$p < 0.005$, ***$p < 0.0005$, ****$p < 0.0001$. GZMB, granzyme B.

transcriptional states (Fig. 2D), we did detect stimulus-specific gene expression patterns, with anti-CD3/CD28 robustly upregulating *GZMB*, *PRF1*, *IFNG*, *IL2RA*, *BATF3*, *CTLA4*, and *LAG3*. In contrast, 5-OP-RU induced a strong type 1 IFN signaling signature with upregulation of *IFIT1*, *ISG15*, *IFI44L*, *IFIT3*, *IFITM1*, and *IFI6*. These findings are consistent with distinct MAIT cell transcriptional programs driven by early Ag-specific signals versus nonspecific T cell stimulation.

MAIT cells upregulate FOXP3 during early and prolonged activation

Given detection of *FOXP3* transcripts across clusters and significant differential expression in C1, we further characterized the transcriptional programs associated with MAIT cell FOXP3 expression using our single-cell data. We first performed a differential expression analysis between FOXP3$^+$ and FOXP3$^-$ MAIT cells in the resting condition at day 1 (Supplemental Fig. 4A, Supplemental Data Set 4) that revealed FOXP3$^+$ MAIT cells differentially express CD4 in addition to markers of activation/exhaustion including TIGIT, ENTPD1, and ICOS, together with IL-2RA, a hallmark of the conventional regulatory T cell (Treg) lineage (44).

We next hypothesized that FOXP3 expression in MAIT cells was associated with acquisition of a transcriptome that might resemble conventional Tregs. To evaluate this, we assembled a list of four conventional Treg gene signatures published by Miragaia et al. (45). In this paper, the authors constructed gene signatures of four Treg populations spanning brachial and mesenteric lymph nodes, colon, and spleen, and established broad conservation of Treg identity between mice and humans. Using these gene signatures, we performed gene set enrichment analysis using the differentially expressed genes from Supplemental Fig. 4A and observed positive enrichment (normalized enrichment score > 0) in all four cases (Supplemental Fig. 4B, 4C, Supplemental Data Set 4). These analyses reveal that resting FOXP3$^+$ MAIT cells differentially express CD4 and are transcriptionally similar to conventional CD4$^+$ Tregs.

We then repeated these analyses using FOXP3$^+$ MAIT cells in the 5-OP-RU condition at day 1. In this case, the cells expressed markers associated with activation and cytotoxicity, for example, CTLA4 and LTB, but were associated with neither CD4 nor CD8 (Supplemental Fig. 4D, Supplemental Data Set 4). In the anti-CD3/CD28 condition, FOXP3$^+$ MAITs also differentially expressed CD4 as well as effector markers similar to the 5-OP-RU–activated condition (Supplemental Fig. 4E, Supplemental Data Set 4). In all conditions, the gene signatures of FOXP3$^+$ MAITs overlapped with signatures of conventional Tregs from the four tissues evaluated in Miragaia et al. (45).

We then applied these analyses to day 7 data. FOXP3$^+$ MAIT cells in the resting condition again demonstrated differential expression of CD4 (Supplemental Fig. 4F, Supplemental Data Set 4) and also expressed activation/effector markers such as GZMB, MKI67, HLA-DR, and TNFRSF18. In contrast, 5-OP-RU–activated FOXP3$^+$ MAITs differentially expressed CD8 together with GZMB, TIGIT, NKG7, and GNLY (Supplemental Fig. 4G, Supplemental Data Set 4). FOXP3$^+$ MAITs in the anti-CD3/CD28 condition were not associated with CD4 or CD8 expression (Supplemental Fig. 4H, Supplemental Data Set 4). As at day 1, gene signatures for FOXP3$^+$ MAITs at day 7 were shared with the

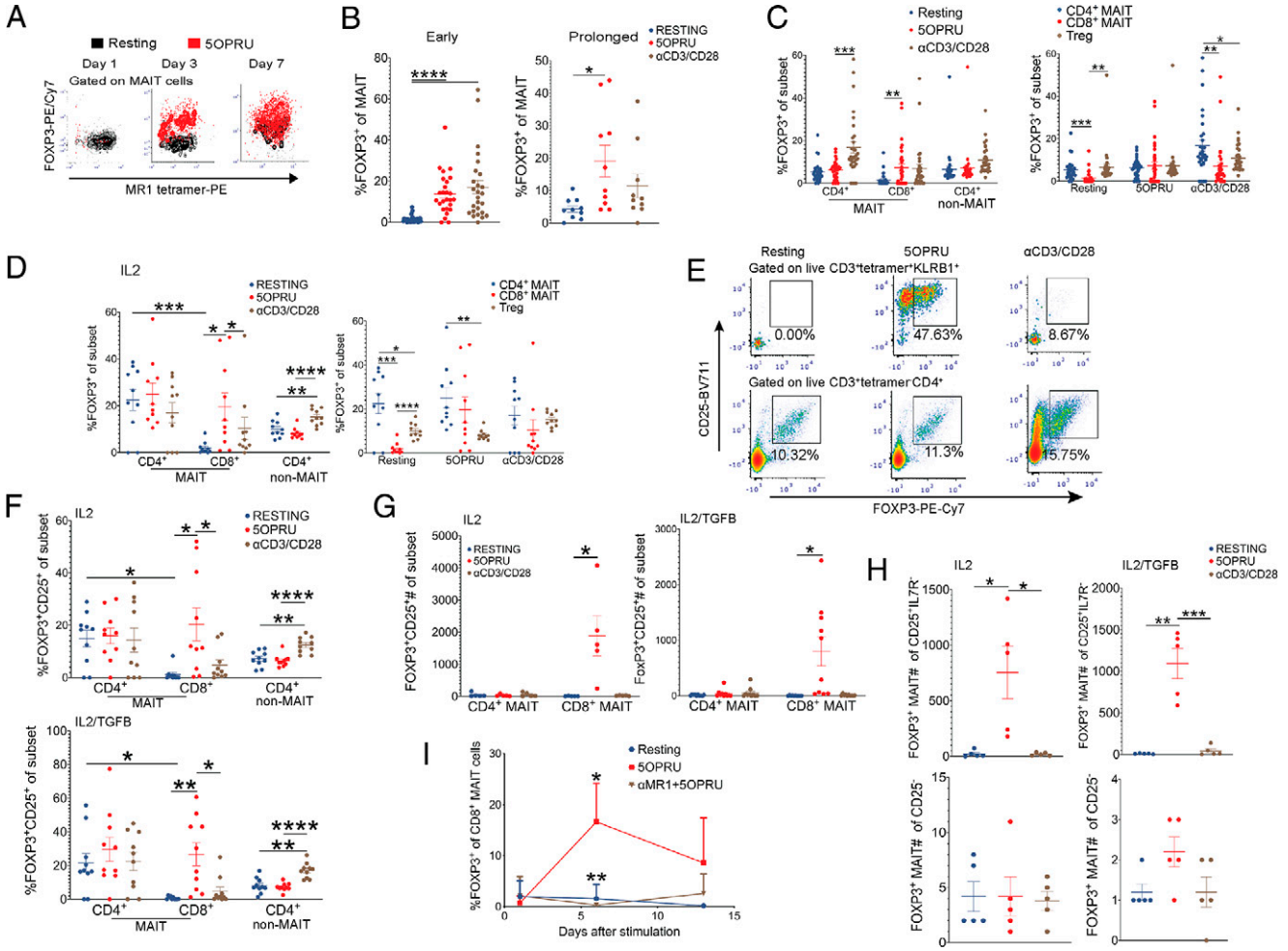

FIGURE 4. MAIT cells upregulate FOXP3 during early and prolonged activation. (**A**) Representative flow cytometry contour plots of MAIT cell FOXP3 intracellular staining in resting or 5-OP-RU conditions after 1, 3, or 7 d of stimulation (black indicates resting; red indicates 5-OP-RU). (**B**) Mean % ± SEM of intracellular MAIT cell FOXP3 staining after 1 (early) or 7 (prolonged) days of incubation under resting (blue), 5-OP-RU (red), or anti-CD3/CD28 (brown) conditions. Results represent three independent experiments. n = 10–26 donors. (**C**) Mean % ± SEM of intracellular FOXP3 staining in CD4$^+$ and CD8$^+$ MAIT cells compared with non-MAIT CD4$^+$ T cells after 15 h of incubation in the same conditions as (B). The same data are grouped by cell type (left) or stimulation condition (right). Results represent two independent experiments. n = 10–26 donors. (**D**) Mean % ± SEM of intracellular FOXP3 staining in CD4$^+$ and CD8$^+$ MAIT cells compared with non-MAIT CD4$^+$ T cells after 7 d of incubation in the same conditions as (B). The same data are grouped by cell type (left) or stimulation condition (right). Results represent two independent experiments. n = 10 donors. (**E**) Representative flow cytometry density plots from one donor demonstrating FOXP3$^+$CD25$^+$ MAIT cells (top row) or non-MAIT CD4$^+$ T cells (bottom row) after 7 d of incubation in the same conditions as (D). (**F**) Mean % ± SEM of FOXP3$^+$CD25$^+$ CD4$^+$ or CD8$^+$ MAIT cells compared with non-MAIT CD4$^+$ T cells after 7 d in the same conditions as (D). Cytokine coincubation conditions included IL-2 (top) or IL-2/TGF-β (bottom). Results represent two independent experiments. n = 10 donors. (**G**) Mean absolute number ± SEM of FOXP3$^+$CD25$^+$ CD4$^+$ or CD8$^+$ MAIT cells in the same incubation conditions as (F). Each condition included 200,000 PBMCs. Results are representative of two independent experiments. n = 5 donors. (**H**) Mean absolute number ± SEM of FOXP3$^+$ MAIT cells among CD25$^+$IL-7R$^-$ MAIT cells or CD25$^-$ MAIT cells after 7 d in the same incubation conditions as (F). Results are representative of two independent experiments. n = 5 donors. Flow cytometric statistical comparisons were made by an unpaired t test, and reported p values are adjusted for multiple comparisons using the Holm–Sidak method. *$p < 0.05$, **$p < 0.005$, ***$p < 0.0005$, ****$p < 0.0001$. (**I**) CD8$^+$ MAIT cell FOXP3 expression under resting, 5-OP-RU, or anti-MR1 blockade/5-OP-RU conditions measured for 2 wk after initial stimulation at day 0. n = 5 donors. All conditions included 100 IU/ml IL-2 and 1 ng/ml TGF-β. Results are representative of two independent experiments. *$p < 0.05$ is the result of an unpaired t test between the 5-OP-RU and resting condition, and **$p < 0.005$ is the result of an unpaired t test between the 5-OP-RU and anti-MR1/5-OP-RU condition.

Miragaia et al. (45) signatures for conventional Tregs. These results demonstrate that FOXP3 expression on $CD4^+$ or $CD8^+$ MAIT cells differs based on antigenic versus nonspecific TCR stimuli. Our data also show that $FOXP3^+$ MAITs at day 7 demonstrate a pronounced cytotoxic effector phenotype, similar to one recent report (23).

To validate the $FOXP3^+$ MAIT cell phenotypes revealed by scRNA-seq, we performed intracellular staining for FOXP3 and flow cytometric analysis stratified by CD4 or CD8 coexpression (Fig. 4) compared with conventional Tregs. As FOXP3 is a transcriptional regulator of conventional $CD4^+$ Tregs and is often coexpressed with CD25 (46, 47), we hypothesized that MAIT cells could share similar staining characteristics. We found that FOXP3 protein was significantly upregulated with Ag-specific stimulation (Fig. 4A, 4B). When we stratified MAIT cells by CD4 or CD8 coexpression at day 1, we observed that $CD4^+$ MAIT cells express more FOXP3 at baseline whereas $CD8^+$ MAIT cells significantly upregulated FOXP3 protein after 5-OP-RU stimulation (Fig. 4C).

As FOXP3 may be transiently upregulated after activation, we also profiled FOXP3 protein expression at day 7 (Fig. 4D–H). Whereas $CD4^+$ MAIT cells had increased FOXP3 expression in the resting condition, consistent with day 1, 5-OP-RU–activated $CD8^+$ MAIT cells robustly upregulated FOXP3 (Fig. 4D). We next compared FOXP3/CD25 coexpression in MAIT cells compared with Tregs and found that 5-OP-RU–activated MAIT cells strongly upregulated these markers of the conventional Treg lineage (Fig. 4E). Direct comparison of CD4 and CD8 expression in $FOXP3^+CD25^+$ by the stimulation condition revealed that coreceptor expression was dependent on the stimulus used (Fig. 4F), in agreement with the single-cell analysis (Supplemental Fig. 4). $CD4^+$ MAIT cells expressed increased FOXP3 and CD25 in the resting condition relative to $CD8^+$ MAIT cells but did not significantly upregulate these markers after prolonged activation (Fig. 4F). In contrast to $CD4^+$ MAIT and conventional Tregs, FOXP3 and CD25 were robustly upregulated in the $CD8^+$ MAIT cell subset after 5-OP-RU activation (Fig. 4F). The addition of TGF-β did not significantly affect MAIT cell FOXP3 expression. As previously reported (48), anti-CD3/CD28 stimulation alone resulted in significant Treg expansion (Fig. 4F). Analysis of absolute numbers of $FOXP3^+CD25^+$ MAIT cells at day 7 demonstrated that $FOXP3^+CD25^+$ MAIT cells were most prevalent within the $CD8^+$ MAIT cell subset (Fig. 4G) and that the vast majority of FOXP3-expressing cells were detected among $CD25^+$IL-$7R^-$ cells and rarely among $CD25^-$ cells (Fig. 4H). We also found that FOXP3 expression in $CD8^+$ MAIT cells of some donors is sustained in some donors for 2 wk following a single Ag-specific stimulation, a phenotype that was dependent on MR1 (Fig. 4I). Taken together, these results demonstrate that FOXP3 is expressed in $CD4^+$ and $CD8^+$ MAIT cells and is associated with distinct stimulatory conditions for each subset. In our attempts to document the functional properties of $FOXP3^+$ MAIT cells, we observed significant interindividual variability in suppression assays (data not shown), and thus we cannot draw any firm conclusions whether FOXP3 expression by MAIT cells is accompanied by suppressive capacity.

Prolonged activation of MAIT cells expands homeostatic subpopulations while also inducing proliferative, cytotoxic, regulatory, and exhausted phenotypes

We next examined clusters enriched during prolonged activation (Fig. 5A). These clusters were broadly associated with expression of *MKI67*, *GZMA*, *CTLA4*, *ICOS*, *LAG3*, and *PDCD1* (Figs. 2, 5A, 5B). Despite largely overlapping transcriptional states observed between prolonged 5-OP-RU and anti-CD3/CD28 conditions (Fig. 2E), 5-OP-RU significantly upregulated genes associated with lymphoid development (*LTB*), self-renewal (*LST1*), maturation (*CD52*), motility and proliferation (*STMN1*, *ACTG1*), and recruitment of immune cells (*CCL3*, *CCL4*). In contrast, anti-CD3/CD28 upregulated genes were associated with cytotoxicity (*GZMB*, *GZMK*), cell stress (*HILPDA*), and exhaustion (*CTLA4*, *LAG3*). This granzyme/exhaustion signature observed was largely driven by C12 defined by cells from donor 1 (Supplemental Fig. 1I).

The transcriptional differences between stimuli were further elucidated at the protein level, where proliferation marker Ki67 was significantly upregulated in the 5-OP-RU but not the anti-CD3/CD28 condition (Fig. 5C). This was consistent with robust Ag-specific MAIT cell expansion not observed with prolonged anti-CD3/CD28 (Fig. 5D, Supplemental Fig. 1B). In contrast, sorted MAIT cells alone stimulated with 5-OP-RU do not significantly expand (49), demonstrating the requirement for accessory cells for proliferation, similar to observations made in γδ T cells (50).

Similar to early activation, we again detected significant downregulation of IL-7R at the protein level only in the 5-OP-RU condition, which was associated with significant upregulation of CD25 not observed with prolonged anti-CD3/CD28 stimulation (Fig. 5E). Similar to early activation, GZMB was the dominant MAIT cell effector protein (Fig. 5F). Activation/exhaustion markers CTLA4, PD1, FAS, ICOS, and LAG3 expression levels were also enhanced with prolonged 5-OP-RU stimulation at the protein level (Fig. 5G).

MAIT cell subtypes are present during human TB exposure and infection

To determine whether MAIT cell subtypes revealed by scRNA-seq are present during human infection, we assessed functional markers associated with $CD4^+$ or $CD8^+$ MAIT cells during human exposure to *Mycobacterium tuberculosis*. To this end, we used flow cytometry to analyze MAIT cell phenotypes in PBMCs collected from household contacts of active TB patients in Port-au-Prince, Haiti compared with healthy unexposed donors from the same community (3).

First, we focused our analysis on a subset of markers that characterized $CD4^+$ MAIT cells in our single-cell analyses. We observed a similar differential expression pattern of CD25, CCR7, and OX40 at the protein level in $CD4^+$ MAIT cells relative to other subsets (Fig. 6A–C). Moreover, each of these markers was significantly upregulated in contacts, indicating that the $CD4^+$ MAIT cell gene expression pattern observed in our clusters in vitro corresponds to in vivo MAIT cell subsets in the context of recent *M. tuberculosis* exposure. Consistent with our previous work (3), these findings indicate that $CD4^+$ MAIT cells respond to early *M. tuberculosis* exposure.

We next investigated MAIT cell FOXP3 expression, which was predominant in the $CD8^+$ subset after in vitro prolonged antigenic stimulation (Fig. 4). We found that recently exposed contacts expressed increased FOXP3 relative to healthy controls (Fig. 6D). Consistent with our flow cytometry results at day 7 (Fig. 4G), $FOXP3^+CD25^+$ MAIT cells were most prevalent in the $CD8^+$ subset, and $FOXP3^+CD25^+CD8^+$ MAIT cells were significantly enriched in contacts (Fig. 6E). When stratifying by *M. tuberculosis*–specific IFN-γ release assay (IGRA) status, which distinguishes contacts who were exposed and latently infected ($IGRA^+$) from those who remained uninfected ($IGRA^-$), we observed that $FOXP3^+CD25^+CD8^+$ MAIT cells were enriched in latently infected contacts (Fig. 6F), demonstrating that this MAIT cell subtype is responding to *M. tuberculosis* infection. This MAIT cell subpopulation detected in TB contacts closely resembles the $CD8^+FOXP3^+CD25^+$ MAIT cells detected at the transcript and protein level at day 7 following Ag-specific stimulation (Fig. 4,

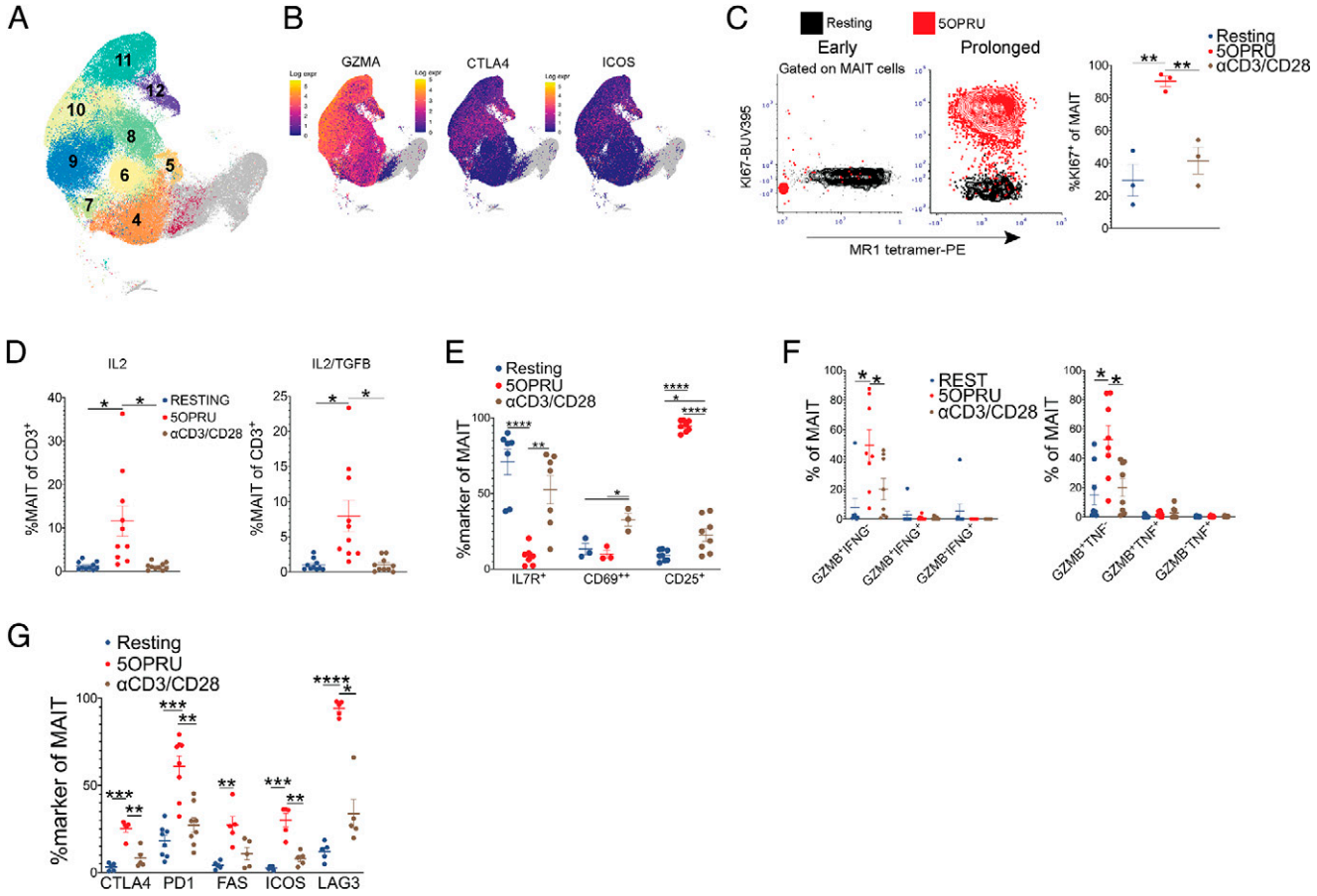

FIGURE 5. Prolonged activation of MAIT cells expands homeostatic subpopulations while also inducing proliferative, cytotoxic, immune regulatory, and exhaustion phenotypes. (**A**) UMAP highlighting clusters 4–12 defined by day 7 incubation conditions. (**B**) UMAP plots of GZMA, CTLA4, and ICOS expression levels at day 7 (blue = low expression to yellow = high expression). (**C**) Representative flow cytometry contour plots (left) of intracellular Ki67 staining after 15 h (day 1; early) or 7 d (day 7; prolonged) of incubation at rest (black) or with 5OPRU (red) accompanied by cumulative data of mean % ± SEM of MAIT cell Ki67 staining after 7 d of incubation under resting (blue), 5OPRU (red), or anti-CD3/CD28 (brown) conditions (right). Results represent one independent experiment. $n = 3$ donors. (**D**) Mean % ± SEM of MAIT cells among total T cells after 7 d of incubation in the same conditions as (C). Results represent two independent experiments. $n = 10$ donors. (**E**) Mean % ± SEM of MAIT cell surface activation markers after 7 d of incubation in the same conditions as (C). Results represent two independent experiments. $n = 3$–8 donors. (**F**) GZMB, IFNG, and TNF intracellular costaining demonstrating mean % ± SEM of each subset after 7 d of incubation under the same conditions as (C). Results represent two independent experiments. $n = 8$ donors. (**G**) Mean % ± SEM of activation/exhaustion marker staining after 7 d of incubation under the same conditions as (C). Results represent one independent experiment. $n = 5$ donors. Flow cytometric statistical comparisons were made by an unpaired t test, and reported p values are adjusted for multiple comparisons using the Holm–Sidak method. $^{*}p < 0.05$, $^{**}p < 0.005$, $^{***}p < 0.0005$, $^{****}p < 0.0001$. GZMB, granzyme B.

Supplemental Fig. 4) and indicates that these cell states defined by single-cell transcriptomics are also present during early human *M. tuberculosis* exposure and infection.

Discussion

MAIT cells have been well characterized as innate-like, rapid responders to microbial Ags with the capacity to mount cytotoxic responses and secrete Th1 helper/Th17-associated cytokines within hours of Ag recognition (3, 9, 39). However, less is known about the transcriptional programs that define MAIT cell adaptation during early and prolonged activation states. In this study, we provide a single-cell transcriptional atlas of >76,000 human MAIT cells in homeostatic and early/prolonged activation states coupled with flow cytometric and functional characterization. Our analysis demonstrates distinct transcriptional programs defined by incubation period and quality of stimulus, revealing novel MAIT cell subpopulations not yet described by bulk RNA-seq or traditional flow cytometric approaches.

First, our work contributes further evidence to support divergent transcriptional and functional phenotypes associated with human MAIT cell CD4 or CD8 coexpression. Several prior studies have used CD8 as a prerequisite for defining MAIT cells or did not distinguish between subsets (21, 22, 51). Differential expression analysis revealed that $CD4^+$ MAIT cells upregulated *IL7R*, *CD25*, *CCR7*, and *SELL* along with TNF superfamily receptors *TNFRSF4* and *TNFRSF18*, suggesting that $CD4^+$ MAIT cells respond to distinct costimulatory signals from the $CD8^+$ subset. We hypothesize that this $CD4^+$ MAIT cell signature may represent unique tissue-homing functions through *CCR7* and *SELL*. Future studies will help to evaluate whether this $CD4^+$ MAIT cell signature confers the capacity to exit the circulation and migrate into tissues.

Recent work in mice and humans shows that CD4 and the transcription factor LEF1 are coexpressed during MAIT cell intrathymic development with reciprocal downregulation of CD319 (SLAMF7) (21). CD4 is subsequently downregulated as MAIT cells mature with reciprocal upregulation of CD8 and CD319 during thymic egress. In a parallel observation in human peripheral blood MAIT

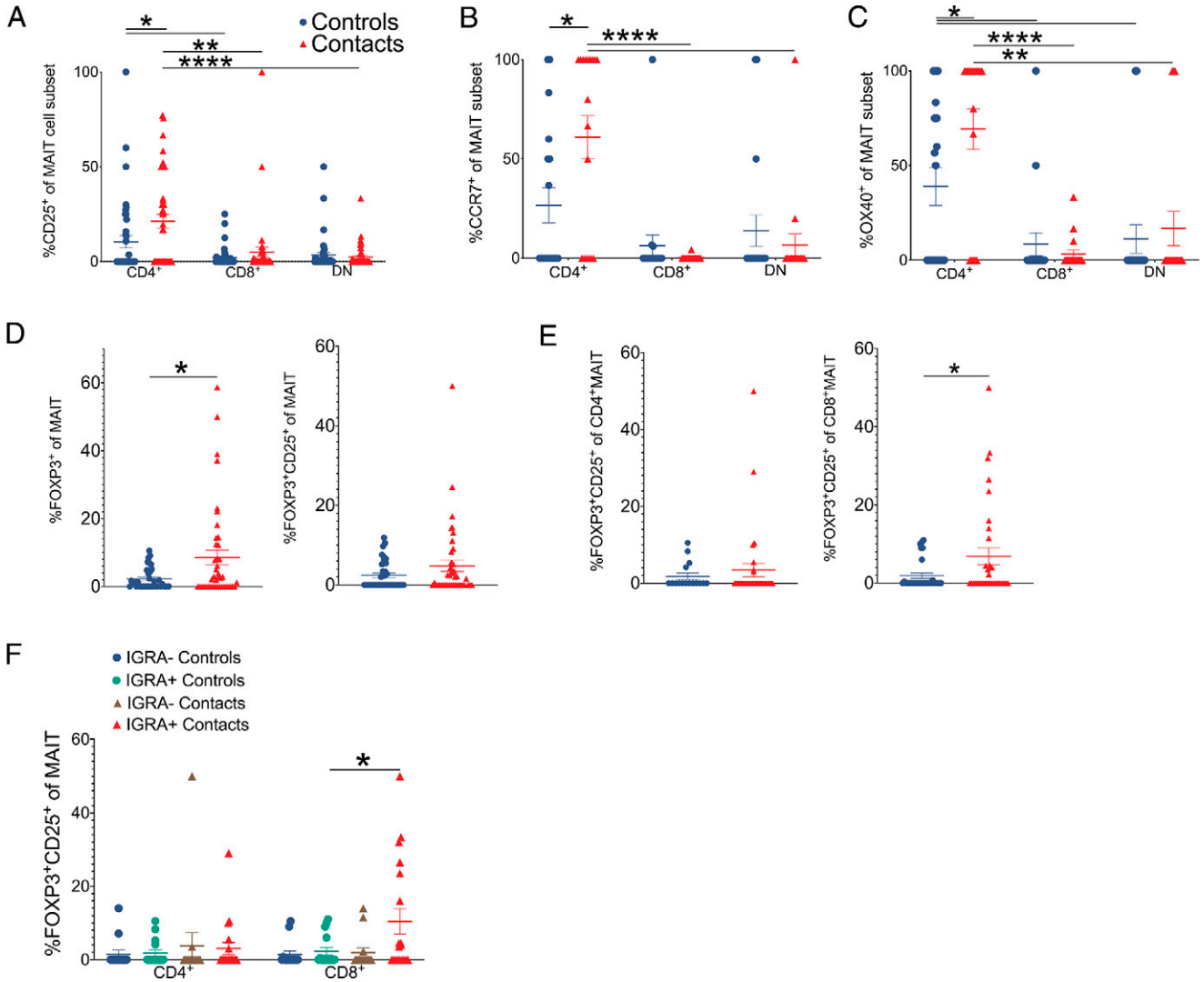

FIGURE 6. MAIT cell subsets differentially respond to *M. tuberculosis*. (**A**–**C**) Mean % ± SEM of CD25 (A), CCR7 (B), and OX40 (C) staining of $CD4^+$, $CD8^+$, or DN MAIT cell subsets in healthy household contacts of TB patients (red triangles) compared with healthy unexposed community controls (blue circles). The same legend also applies to (**D**) and (**E**). Results represent more than three independent experiments. $n = 18$–41 donors. (D) Mean % ± SEM of $FOXP3^+$ (left) or $FOXP3^+CD25^+$ (right) MAIT cells. Results represent more than three independent experiments. $n = 36$–42 donors. (E) Mean % ± SEM of $FOXP3^+CD25^+$ $CD4^+$ (left) or $CD8^+$ MAIT cells (right) in the same donors as (D). (**F**) Mean % ± SEM of $FOXP3^+CD25^+$ $CD4^+$ or $C8^+$ MAIT cells stratified by IGRA status in the same donors as (D). Flow cytometric statistical comparisons were made by Mann–Whitney *U* test in (A)–(C) or unpaired *t* test panels (D)–(F), and reported *p* values are adjusted for multiple comparisons using the Holm–Sidak method. $*p < 0.05$, $**p < 0.005$, $***p < 0.0005$, $****p < 0.0001$. IGRA, *M. tuberculosis*–specific IFN-γ release assay.

cells, we observed that $CD4^+$ MAIT cells significantly upregulated *LEF1*, whereas *SLAMF7* was significantly differentially expressed in $CD8^+$ MAIT cells. Our findings motivate additional study of how MAIT cell activation conditions can select for CD4 or CD8 coexpression in peripheral circulating populations, and, further, how these subsets differentially respond to major pathogens. Indeed, our TB contact data demonstrate that CD25, CCR7, and OX40 are significantly upregulated in $CD4^+$ MAIT cells and FOXP3 in $CD8^+$ MAIT cells of TB contacts, suggesting that these subsets respond to early *M. tuberculosis* exposure.

The second aim of our study was to distinguish between transcriptional phenotypes induced during early and prolonged activation and to characterize functional programs associated with MR1 ligand versus nonspecific T cell stimulation. We observed that early activated MAIT cells with either stimulus were driven toward similar states defined by a rapid upregulation of GZMB, IFN-γ, and TNF-α. At both the transcript and protein levels, this signature was more potently induced by anti-CD3/CD28, which is possibly explained by nonspecific stimulation of all T cells within PBMCs triggering cytokine release by MAIT and non-MAIT T cells alike (52). Moreover, anti-CD3/CD28 may mimic other nonspecific T cell stimuli derived from whole bacteria or cytokines, which have previously been shown to significantly upregulate GZMB and IFN-γ in MAIT cells relative to 5-OP-RU alone (12, 43). We acknowledge that our study design could not identify the additional inflammatory signals induced by anti-CD3/CD28 stimulation compared with MR1 ligand (22) nor quantify MR1 expression by specific immune subsets within the PBMC aliquot. Future studies will identify which accessory cell types (53) and costimulatory conditions (38, 54) drive activation of specific MAIT cell subpopulations in healthy and disease states. In contrast to nonspecific TCR stimulation, early activation with 5-OP-RU induced a strong type 1 IFN–driven gene expression phenotype along with T cell maturation marker CD52. Costimulation of MAIT cells with 5-OP-RU and type 1 IFNs have

previously been shown to enhance GZMB and IFN-γ release (54). Our results demonstrate that early Ag stimulation alone also enhances MAIT cell type 1 IFN signaling as detected at the transcript level in our scRNA-seq dataset, which may promote survival and proliferation observed during prolonged stimulation (55) as well as modulate immunity against bacterial or viral pathogens (56).

Although previous studies have used prolonged 5-OP-RU costimulation to expand MAIT cells for downstream use during in vitro functional assays (49, 57), to our knowledge, this is the first investigation of the transcriptional landscape of prolonged Ag-specific activation during this proliferative phase. Although we observed largely overlapping transcriptional signatures between 5-OP-RU and anti-CD3/CD28 activation conditions, 5-OP-RU significantly upregulated genes associated with T cell development, self-renewal, proliferation, and recruitment of inflammatory cells. In contrast, prolonged anti-CD3/CD28 activation upregulated genes associated with cytotoxicity, stress, and exhaustion. Taken together, these results demonstrate that Ag-specific stimulation is required for MAIT cell survival, expansion, and sustained effector function during the prolonged phase of stimulation.

Moreover, we describe a $FOXP3^+$ peripheral blood MAIT cell subset enriched in early activation C1 with abundant FOXP3 detected at the protein level during prolonged 5-OP-RU stimulation. We observed that $CD4^+$ MAIT cells expressed increased FOXP3 in the resting state relative to the $CD8^+$ subset, similar to a recent study that detected tumor-associated $FOXP3^+CD4^+$ MAIT cells (23). We also demonstrate that peripheral $FOXP3^+$ induction was detected almost exclusively in the $CD8^+CD25^+IL\text{-}7R^-$ subset after Ag-specific induction. This surface coexpression of FOXP3 and CD25 in MAIT cells parallels that of $CD4^+$ Tregs and raises the question of whether FOXP3 expression in MAIT cells may confer a similar immune regulatory function (32). We observed considerable interindividual variability in our MAIT cell suppression assays and thus cannot draw firm conclusions regarding MAIT cell regulatory function at this time. Further study is required to investigate the suppressive capacity of $FOXP3^+$ MAIT cells. Importantly, we extend our findings of MAIT cell FOXP3 induction in vitro to immune responses of donors recently exposed to *M. tuberculosis*. We found that $CD8^+FOXP3^+CD25^+$ MAIT cells expanded after early *M. tuberculosis* exposure in healthy household TB contacts and were significantly more abundant in recently infected donors ($IGRA^+$ contacts). Our results suggest that $CD8^+FOXP3^+CD25^+$ MAIT cells expand during early *M. tuberculosis* infection.

Our study also highlights that MAIT cell activation rapidly drives expression of phenotypic exhaustion markers. This was evident in both Ag and nonspecific stimulation conditions at the transcriptional and protein levels. These findings mirror evidence from chronic disease states such as TB, viral hepatitis, and malignancy where increased MAIT cell PD1 expression is associated with peripheral MAIT cell depletion and dysfunction and directly correlates with severity of disease in some studies (11, 58–64). Although immune checkpoint molecules can be transiently upregulated after T cell activation, we observed sustained expression in prolonged activation clusters. At the protein level, these exhaustion markers were significantly upregulated in the 5-OP-RU condition, suggesting that prolonged Ag-specific activation strongly induces negative feedback mechanisms to suppress further activation and proliferation. Taken together, these data imply that checkpoint blockade may enhance MAIT cell activity against infectious or malignant disease (57, 65, 66) or contribute to autoimmune complications of immunotherapy (67).

Given the recently described importance of MAIT cells in SARS-CoV-2 pathogenesis (24, 25, 68), we also show that MAIT cell transcriptional markers in severe COVID-19 disease are expressed in distinct MAIT cell clusters defined in the present study (Supplemental Fig. 2F). The MAIT cell subtypes identified in this study may provide additional refinement into the pathologic role of MAIT cell subpopulations in COVID-19 disease severity.

We acknowledge certain limitations to our study. The foremost of these is the small number of individuals in our single-cell cohort and donor-to-donor variability, some of which is inherent in human studies from genetically diverse subjects. However, the functional flow cytometric validation in multiple donors, including a genetically distinct population from Haiti, strengthens our confidence that the MAIT cell states observed can be applied to other populations. Future studies will test the reproducibility of this transcriptional atlas in additional healthy donors or in specific disease states.

In sum, we present an integrated transcriptional and immune landscape of human MAIT cell activation at single-cell resolution. Our results provide a detailed analysis of novel MAIT cell clusters defined by early and prolonged stimulation, including distinct $CD4^+$ and $CD8^+$ MAIT cell signatures. We also show that these phenotypes are recapitulated in the setting of early *M. tuberculosis* exposure and infection. This functional map of MAIT cell activation biology will help inform future investigations into how MAIT cells specialize in healthy and disease states.

Acknowledgments

We thank Ojasvi Chaudhury for assistance in preparation of single-cell RNA-seq libraries. We acknowledge staff at the Immune Monitoring, Flow Cytometry, and Integrated Genomics Operation Core Facilities at the Sloan Kettering Institute, Memorial Sloan-Kettering Cancer (New York, NY) for expert consultation and services rendered during this project. We also acknowledge the National Institutes of Health Tetramer Core (Emory University, Atlanta, GA) for providing MR1 tetramers.

Disclosures

M.S.G. reports consulting fees and equity in Vedanta Biosciences, Inc., is a consultant for Fimbrion, and is on the Scientific Advisory Board of PRL-NYC. The other authors have no financial conflicts of interest.

References

1. Godfrey, D. I., H. F. Koay, J. McCluskey, and N. A. Gherardin. 2019. The biology and functional importance of MAIT cells. *Nat. Immunol.* 20: 1110–1128.
2. Li, K., C. K. Vorkas, A. Chaudhry, D. L. Bell, R. A. Willis, A. Rudensky, J. D. Altman, M. S. Glickman, and J. Aubé. 2018. Synthesis, stabilization, and characterization of the MR1 ligand precursor 5-amino-6-D-ribitylaminouracil (5-A-RU). *PLoS One* 13: e0191837.
3. Vorkas, C. K., M. F. Wipperman, K. Li, J. Bean, S. K. Bhattarai, M. Adamow, P. Wong, J. Aubé, M. A. J. Juste, V. Bucci, et al. 2018. Mucosal-associated invariant and γδ T cell subsets respond to initial *Mycobacterium tuberculosis* infection. *JCI Insight* 3: e121899.
4. Harriff, M. J., C. McMurtrey, C. A. Froyd, H. Jin, M. Cansler, M. Null, A. Worley, E. W. Meermeier, G. Swarbrick, A. Nilsen, et al. 2018. MR1 displays the microbial metabolome driving selective MR1-restricted T cell receptor usage. *Sci. Immunol.* 3: eaao2556.
5. Treiner, E., L. Duban, S. Bahram, M. Radosavljevic, V. Wanner, F. Tilloy, P. Affaticati, S. Gilfillan, and O. Lantz. 2003. Selection of evolutionarily conserved mucosal-associated invariant T cells by MR1. [Published erratum appears in 2003 *Nature* 423: 1018.] *Nature* 422: 164–169.
6. Seshadri, C., N. T. Thuong, N. T. Mai, N. D. Bang, T. T. Chau, D. M. Lewinsohn, G. E. Thwaites, S. J. Dunstan, and T. R. Hawn. 2017. A polymorphism in human MR1 is associated with mRNA expression and susceptibility to tuberculosis. *Genes Immun.* 18: 8–14.
7. Legoux, F., D. Bellet, C. Daviaud, Y. El Morr, A. Darbois, K. Niort, E. Procopio, M. Salou, J. Gilet, B. Ryffel, et al. 2019. Microbial metabolites control the thymic development of mucosal-associated invariant T cells. *Science* 366: 494–499.
8. Kaech, S. M., and R. Ahmed. 2001. Memory $CD8^+$ T cell differentiation: initial antigen encounter triggers a developmental program in naïve cells. *Nat. Immunol.* 2: 415–422.
9. Dias, J., E. Leeansyah, and J. K. Sandberg. 2017. Multiple layers of heterogeneity and subset diversity in human MAIT cell responses to distinct microorganisms and to innate cytokines. *Proc. Natl. Acad. Sci. USA* 114: E5434–E5443.
10. Jahreis, S., S. Böttcher, S. Hartung, T. Rachow, S. Rummler, A. M. Dietl, H. Haas, G. Walther, A. Hochhaus, and M. von Lilienfeld-Toal. 2018. Human MAIT cells are rapidly activated by *Aspergillus* spp. in an APC-dependent manner. *Eur. J. Immunol.* 48: 1698–1706.

11. Shaler, C. R., J. Choi, P. T. Rudak, A. Memarnejadian, P. A. Szabo, M. E. Tun-Abraham, J. Rossjohn, A. J. Corbett, J. McCluskey, J. K. McCormick, et al. 2017. MAIT cells launch a rapid, robust and distinct hyperinflammatory response to bacterial superantigens and quickly acquire an anergic phenotype that impedes their cognate antimicrobial function: defining a novel mechanism of superantigen-induced immunopathology and immunosuppression. *PLoS Biol.* 15: e2001930.
12. Lamichhane, R., M. Schneider, S. M. de la Harpe, T. W. R. Harrop, R. F. Hannaway, P. K. Dearden, J. R. Kirman, J. D. A. Tyndall, A. J. Vernall, and J. E. Ussher. 2019. TCR- or cytokine-activated $CD8^+$ mucosal-associated invariant T cells are rapid polyfunctional effectors that can coordinate immune responses. *Cell Rep.* 28: 3061–3076.e5.
13. Leng, T., H. D. Akther, C. P. Hackstein, K. Powell, T. King, M. Friedrich, Z. Christoforidou, S. McCuaig, M. Neyazi, C. V. Arancibia-Cárcamo, et al.; Oxford IBD Investigators. 2019. TCR and inflammatory signals tune human MAIT cells to exert specific tissue repair and effector functions. *Cell Rep.* 28: 3077–3091.e5.
14. van Wilgenburg, B., I. Scherwitzl, E. C. Hutchinson, T. Leng, A. Kurioka, C. Kulicke, C. de Lara, S. Cole, S. Vasanawathana, W. Limpitikul, et al. 2016. MAIT cells are activated during human viral infections. *Nat. Commun.* 7: 11653.
15. Gherardin, N. A., M. N. Souter, H. F. Koay, K. M. Mangas, T. Seemann, T. P. Stinear, S. B. Eckle, S. P. Berzins, Y. d'Udekem, I. E. Konstantinov, et al. 2018. Human blood MAIT cell subsets defined using MR1 tetramers. *Immunol. Cell Biol.* 96: 507–525.
16. Kurioka, A., A. S. Jahun, R. F. Hannaway, L. J. Walker, J. R. Fergusson, E. Sverremark-Ekström, A. J. Corbett, J. E. Ussher, C. B. Willberg, and P. Klenerman. 2017. Shared and distinct phenotypes and functions of human CD161++ Vα7.2+ T cell subsets. *Front. Immunol.* 8: 1031.
17. Dias, J., C. Boulouis, J. B. Gorin, R. H. G. A. van den Biggelaar, K. G. Lal, A. Gibbs, L. Loh, M. Y. Gulam, W. R. Sia, S. Bari, et al. 2018. The $CD4^-CD8^-$ MAIT cell subpopulation is a functionally distinct subset developmentally related to the main $CD8^+$ MAIT cell pool. *Proc. Natl. Acad. Sci. USA* 115: E11513–E11522.
18. Kelly, J., Y. Minoda, T. Meredith, G. Cameron, M. S. Philipp, D. G. Pellicci, A. J. Corbett, C. Kurts, D. H. Gray, D. I. Godfrey, et al. 2019. Chronically stimulated human MAIT cells are unexpectedly potent IL-13 producers. *Immunol. Cell Biol.* 97: 689–699.
19. Gutierrez-Arcelus, M., N. Teslovich, A. R. Mola, R. B. Polidoro, A. Nathan, H. Kim, S. Hannes, K. Slowikowski, G. F. M. Watts, I. Korsunsky, et al. 2019. Lymphocyte innateness defined by transcriptional states reflects a balance between proliferation and effector functions. *Nat. Commun.* 10: 687.
20. Lee, M., E. Lee, S. K. Han, Y. H. Choi, D. I. Kwon, H. Choi, K. Lee, E. S. Park, M. S. Rha, D. J. Joo, et al. 2020. Single-cell RNA sequencing identifies shared differentiation paths of mouse thymic innate T cells. *Nat. Commun.* 11: 4367.
21. Koay, H. F., S. Su, D. Amann-Zalcenstein, S. R. Daley, I. Comerford, L. Miosge, C. E. Whyte, I. E. Konstantinov, Y. d'Udekem, T. Baldwin, et al. 2019. A divergent transcriptional landscape underpins the development and functional branching of MAIT cells. *Sci. Immunol.* 4: eaay6039.
22. Slichter, C. K., A. McDavid, H. W. Miller, G. Finak, B. J. Seymour, J. P. McNevin, G. Diaz, J. L. Czartoski, M. J. McElrath, R. Gottardo, and M. Prlic. 2016. Distinct activation thresholds of human conventional and innate-like memory T cells. *JCI Insight* 1: e86292.
23. Li, S., Y. Simoni, E. Becht, C. Y. Loh, N. Li, D. Lachance, S. L. Koo, T. P. Lim, E. K. W. Tan, R. Mathew, et al. 2020. Human tumor-infiltrating MAIT cells display hallmarks of bacterial antigen recognition in colorectal cancer. *Cell Rep Med* 1: 100039.
24. Parrot, T., J. B. Gorin, A. Ponzetta, K. T. Maleki, T. Kammann, J. Emgard, A. Perez-Potti, T. Sekine, O. Rivera-Ballesteros, C.-S. G. Karolinska, et al. 2020. MAIT cell activation and dynamics associated with COVID-19 disease severity. *Sci. Immunol.* 5: eabe1670.
25. Flament, H., M. Rouland, L. Beaudoin, A. Toubal, L. Bertrand, S. Lebourgeois, C. Rousseau, P. Soulard, Z. Gouda, L. Cagninacci, et al. 2021. Outcome of SARS-CoV-2 infection is linked to MAIT cell activation and cytotoxicity. *Nat. Immunol.* 22: 322–335.
26. Corbett, A. J., S. B. Eckle, R. W. Birkinshaw, L. Liu, O. Patel, J. Mahony, Z. Chen, R. Reantragoon, B. Meehan, H. Cao, et al. 2014. T-cell activation by transitory neo-antigens derived from distinct microbial pathways. *Nature* 509: 361–365.
27. Azizi, E., A. J. Carr, G. Plitas, A. E. Cornish, C. Konopacki, S. Prabhakaran, J. Nainys, K. Wu, V. Kiseliovas, M. Setty, et al. 2018. Single-cell map of diverse immune phenotypes in the breast tumor microenvironment. *Cell* 174: 1293–1308.e36.
28. Haghverdi, L., A. T. L. Lun, M. D. Morgan, and J. C. Marioni. 2018. Batch effects in single-cell RNA-sequencing data are corrected by matching mutual nearest neighbors. *Nat. Biotechnol.* 36: 421–427.
29. Bindea, G., B. Mlecnik, M. Tosolini, A. Kirilovsky, M. Waldner, A. C. Obenauf, H. Angell, T. Fredriksen, L. Lafontaine, A. Berger, et al.2013. Spatiotemporal dynamics of intratumoral immune cells reveal the immune landscape in human cancer. *Immunity* 39: 782–795.
30. Sharma, P. K., E. B. Wong, R. J. Napier, W. R. Bishai, T. Ndung'u, V. O. Kasprowicz, D. A. Lewinsohn, D. M. Lewinsohn, and M. C. Gold. 2015. High expression of CD26 accurately identifies human bacteria-reactive MR1-restricted MAIT cells. *Immunology* 145: 443–453.
31. Lamichhane, R., and J. E. Ussher. 2017. Expression and trafficking of MR1. *Immunology* 151: 270–279.
32. Bhattacharyya, A., L. A. Hanafi, A. Sheih, J. L. Golob, S. Srinivasan, M. J. Boeckh, S. A. Pergam, S. Mahmood, K. K. Baker, T. A. Gooley, et al. 2018. Graft-derived reconstitution of mucosal-associated invariant T cells after allogeneic hematopoietic cell transplantation. *Biol. Blood Marrow Transplant.* 24: 242–251.
33. Rouxel, O., J. Da Silva, L. Beaudoin, I. Nel, C. Tard, L. Cagninacci, B. Kiaf, M. Oshima, M. Diedisheim, M. Salou, et al. 2017. Cytotoxic and regulatory roles of mucosal-associated invariant T cells in type 1 diabetes. [Published erratum appears in 2018 *Nat. Immunol.* 19: 1035.] *Nat. Immunol.* 18: 1321–1331.
34. Sagerström, C. G., E. M. Kerr, J. P. Allison, and M. M. Davis. 1993. Activation and differentiation requirements of primary T cells in vitro. *Proc. Natl. Acad. Sci. USA* 90: 8987–8991.
35. Pritykin, Y., J. van der Veeken, A. R. Pine, Y. Zhong, M. Sahin, L. Mazutis, D. Pe'er, A. Y. Rudensky, and C. S. Leslie. 2021. A unified atlas of CD8 T cell dysfunctional states in cancer and infection. *Mol. Cell* 81: 2477–2493.e10.
36. Meierovics, A., W. J. Yankelevich, and S. C. Cowley. 2013. MAIT cells are critical for optimal mucosal immune responses during in vivo pulmonary bacterial infection. *Proc. Natl. Acad. Sci. USA* 110: E3119–E3128.
37. Lal, K. G., D. Kim, M. C. Costanzo, M. Creegan, E. Leeansyah, J. Dias, D. Paquin-Proulx, L. A. Eller, A. Schuetz, Y. Phuang-Ngern, et al. 2020. Dynamic MAIT cell response with progressively enhanced innateness during acute HIV-1 infection. *Nat. Commun.* 11: 272.
38. Chen, Z., H. Wang, C. D'Souza, S. Sun, L. Kostenko, S. B. Eckle, B. S. Meehan, D. C. Jackson, R. A. Strugnell, H. Cao, et al. 2017. Mucosal-associated invariant T-cell activation and accumulation after in vivo infection depends on microbial riboflavin synthesis and co-stimulatory signals. *Mucosal Immunol.* 10: 58–68.
39. Dusseaux, M., E. Martin, N. Serriari, I. Péguillet, V. Premel, D. Louis, M. Milder, L. Le Bourhis, C. Soudais, E. Treiner, and O. Lantz. 2011. Human MAIT cells are xenobiotic-resistant, tissue-targeted, $CD161^{hi}$ IL-17-secreting T cells. *Blood* 117: 1250–1259.
40. Garner, L. C., P. Klenerman, and N. M. Provine. 2018. Insights into mucosal-associated invariant T cell biology from studies of invariant natural killer T cells. *Front. Immunol.* 9: 1478.
41. Keller, A. N., A. J. Corbett, J. M. Wubben, J. McCluskey, and J. Rossjohn. 2017. MAIT cells and MR1-antigen recognition. *Curr. Opin. Immunol.* 46: 66–74.
42. Dillon, S. R., M. Mancini, A. Rosen, and M. S. Schlissel. 2000. Annexin V binds to viable B cells and colocalizes with a marker of lipid rafts upon B cell receptor activation. *J. Immunol.* 164: 1322–1332.
43. Suliman, S., M. Murphy, M. Musvosvi, A. Gela, E. W. Meermeier, H. Geldenhuys, C. Hopley, A. Toefy, N. Bilek, A. Veldsman, et al. 2019. MR1-independent activation of human mucosal-associated invariant T cells by mycobacteria. *J. Immunol.* 203: 2917–2927.
44. Toomer, K. H., J. B. Lui, N. H. Altman, Y. Ban, X. Chen, and T. R. Malek. 2019. Essential and non-overlapping IL-2Rα-dependent processes for thymic development and peripheral homeostasis of regulatory T cells. *Nat. Commun.* 10: 1037.
45. Miragaia, R. J., T. Gomes, A. Chomka, L. Jardine, A. Riedel, A. N. Hegazy, N. Whibley, A. Tucci, X. Chen, I. Lindeman, et al. 2019. Single-cell transcriptomics of regulatory T cells reveals trajectories of tissue adaptation. *Immunity* 50: 493–504.e7.
46. Liston, A., K. M. Nutsch, A. G. Farr, J. M. Lund, J. P. Rasmussen, P. A. Koni, and A. Y. Rudensky. 2008. Differentiation of regulatory $Foxp3^+$ T cells in the thymic cortex. *Proc. Natl. Acad. Sci. USA* 105: 11903–11908.
47. Yamaguchi, T., J. B. Wing, and S. Sakaguchi. 2011. Two modes of immune suppression by $Foxp3^+$ regulatory T cells under inflammatory or non-inflammatory conditions. *Semin. Immunol.* 23: 424–430.
48. Hoffmann, P., R. Eder, L. A. Kunz-Schughart, R. Andreesen, and M. Edinger. 2004. Large-scale in vitro expansion of polyclonal human $CD4^+CD25^{high}$ regulatory T cells. *Blood* 104: 895–903.
49. Gherardin, N. A., L. Loh, L. Admojo, A. J. Davenport, K. Richardson, A. Rogers, P. K. Darcy, M. R. Jenkins, H. M. Prince, S. J. Harrison, et al. 2018. Enumeration, functional responses and cytotoxic capacity of MAIT cells in newly diagnosed and relapsed multiple myeloma. *Sci. Rep.* 8: 4159.
50. Ribot, J. C., A. deBarros, D. J. Pang, J. F. Neves, V. Peperzak, S. J. Roberts, M. Girardi, J. Borst, A. C. Hayday, D. J. Pennington, and B. Silva-Santos. 2009. CD27 is a thymic determinant of the balance between interferon-γ- and interleukin 17-producing γδ T cell subsets. *Nat. Immunol.* 10: 427–436.
51. Coulter, F., A. Parrish, D. Manning, B. Kampmann, J. Mendy, M. Garand, D. M. Lewinsohn, E. M. Riley, and J. S. Sutherland. 2017. IL-17 production from T helper 17, mucosal-associated invariant T, and γδ cells in tuberculosis infection and disease. *Front. Immunol.* 8: 1252.
52. Trickett, A., and Y. L. Kwan. 2003. T cell stimulation and expansion using anti-CD3/CD28 beads. *J. Immunol. Methods* 275: 251–255.
53. Nerdal, P. T., C. Peters, H. H. Oberg, H. Zlatev, M. Lettau, E. S. Quabius, S. Sousa, D. Gonnermann, S. Auriola, D. Olive, et al. 2016. Butyrophilin 3A/CD277-dependent activation of human γδ T cells: accessory cell capacity of distinct leukocyte populations. *J. Immunol.* 197: 3059–3068.
54. Lamichhane, R., H. Galvin, R. F. Hannaway, S. M. de la Harpe, F. Munro, J. D. Tyndall, A. J. Vernall, J. L. McCall, M. Husain, and J. E. Ussher. 2020. Type I interferons are important co-stimulatory signals during T cell receptor mediated human MAIT cell activation. *Eur. J. Immunol.* 50: 178–191.
55. Welsh, R. M., K. Bahl, H. D. Marshall, and S. L. Urban. 2012. Type 1 interferons and antiviral CD8 T-cell responses. *PLoS Pathog.* 8: e1002352.
56. Trinchieri, G. 2010. Type I interferon: friend or foe? *J. Exp. Med.* 207: 2053–2063.
57. Boulouis, C., W. R. Sia, M. Y. Gulam, J. Q. M. Teo, Y. T. Png, T. K. Phan, J. Y. W. Mak, D. P. Fairlie, I. K. H. Poon, T. H. Koh, et al. 2020. Human MAIT cell cytolytic effector proteins synergize to overcome carbapenem resistance in *Escherichia coli*. *PLoS Biol.* 18: e3000644.
58. Duan, M., S. Goswami, J. Y. Shi, L. J. Wu, X. Y. Wang, J. Q. Ma, Z. Zhang, Y. Shi, L. J. Ma, S. Zhang, et al. 2019. Activated and exhausted MAIT cells foster disease progression and indicate poor outcome in hepatocellular carcinoma. *Clin. Cancer Res.* 25: 3304–3316.

59. Hengst, J., B. Strunz, K. Deterding, H. G. Ljunggren, E. Leeansyah, M. P. Manns, M. Cornberg, J. K. Sandberg, H. Wedemeyer, and N. K. Björkström. 2016. Nonreversible MAIT cell-dysfunction in chronic hepatitis C virus infection despite successful interferon-free therapy. *Eur. J. Immunol.* 46: 2204–2210.
60. Jiang, J., X. Wang, H. An, B. Yang, Z. Cao, Y. Liu, J. Su, F. Zhai, R. Wang, G. Zhang, and X. Cheng. 2014. Mucosal-associated invariant T-cell function is modulated by programmed death-1 signaling in patients with active tuberculosis. *Am. J. Respir. Crit. Care Med.* 190: 329–339.
61. Jiang, J., Z. Cao, J. Qu, H. Liu, H. Han, and X. Cheng. 2020. PD-1-expressing MAIT cells from patients with tuberculosis exhibit elevated production of CXCL13. *Scand. J. Immunol.* 91: e12858.
62. Leeansyah, E., A. Ganesh, M. F. Quigley, A. Sönnerborg, J. Andersson, P. W. Hunt, M. Somsouk, S. G. Deeks, J. N. Martin, M. Moll, et al. 2013. Activation, exhaustion, and persistent decline of the antimicrobial MR1-restricted MAIT-cell population in chronic HIV-1 infection. *Blood* 121: 1124–1135.
63. Saeidi, A., V. L. Tien Tien, R. Al-Batran, H. A. Al-Darraji, H. Y. Tan, Y. K. Yong, S. Ponnampalavanar, M. Barathan, D. V. Rukumani, A. W. Ansari, et al. 2015. Attrition of TCR Vα7.2+ CD161++ MAIT cells in HIV-tuberculosis co-infection is associated with elevated levels of PD-1 expression. *PLoS One* 10: e0124659.
64. Yong, Y. K., A. Saeidi, H. Y. Tan, M. Rosmawati, P. F. Enström, R. A. Batran, V. Vasuki, I. Chattopadhyay, A. Murugesan, R. Vignesh, et al. 2018. Hyper-expression of PD-1 is associated with the levels of exhausted and dysfunctional phenotypes of circulating $CD161^{++}$TCR $iV\alpha7.2^{+}$ mucosal-associated invariant T cells in chronic hepatitis B virus infection. *Front. Immunol.* 9: 472.
65. Leeansyah, E., J. Svärd, J. Dias, M. Buggert, J. Nyström, M. F. Quigley, M. Moll, A. Sönnerborg, P. Nowak, and J. K. Sandberg. 2015. Arming of MAIT cell cytolytic antimicrobial activity is induced by IL-7 and defective in HIV-1 infection. *PLoS Pathog.* 11: e1005072.
66. Venken, K., M. Favreau, D. Gaublomme, E. Menu, K. Vanderkerken, and D. Elewaut. 2018. Checkpoint inhibition in the treatment of multiple myeloma: a way to boost innate-like T cell anti-tumor function? *Mol. Immunol.* 101: 521–526.
67. Sasson, S. C., J. J. Zaunders, K. Nahar, C. M. L. Munier, B. P. Fairfax, A. Olsson-Brown, C. Jolly, S. A. Read, G. Ahlenstiel, U. Palendira, et al. 2020. Mucosal-associated invariant T (MAIT) cells are activated in the gastrointestinal tissue of patients with combination ipilimumab and nivolumab therapy-related colitis in a pathology distinct from ulcerative colitis. *Clin. Exp. Immunol.* 202: 335–352.
68. Deschler, S., J. Kager, J. Erber, L. Fricke, P. Koyumdzhieva, A. Georgieva, T. Lahmer, J. R. Wiessner, F. Voit, J. Schneider, et al. 2021. Mucosal-associated invariant T (MAIT) cells are highly activated and functionally impaired in COVID-19 patients. *Viruses* 13: 241.